

# Cardiolipin Promotes Pore-Forming Activity of Alpha-Synuclein Oligomers in Mitochondrial Membranes

Stephanie Ghio,<sup>†</sup> Angelique Camilleri,<sup>†</sup> Mario Caruana,<sup>†</sup> Viktoria C. Ruf,<sup>‡,§</sup> Felix Schmidt,<sup>‡</sup> Andrei Leonov,<sup>§</sup> Sergey Ryazanov,<sup>§,#</sup> Christian Griesinger,<sup>§,¶</sup> Ruben J. Cauchi,<sup>†</sup> Frits Kamp,<sup>¶</sup> Armin Giese,<sup>‡</sup> and Neville Vassallo<sup>\*,†,§</sup>

<sup>†</sup>Department of Physiology and Biochemistry and Centre for Molecular Medicine and Biobanking, University of Malta, Msida, Malta

<sup>‡</sup>Center for Neuropathology and Prion Research, Ludwig-Maximilians-University, Munich, Germany

<sup>§</sup>Department of NMR-based Structural Biology, Max Planck Institute for Biophysical Chemistry, Göttingen, Germany

<sup>#</sup>MODAG GmbH, Wendelsheim, Germany

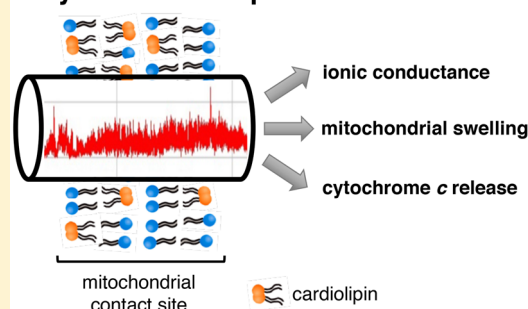
<sup>¶</sup>Biomedical Center, Metabolic Biochemistry, Ludwig-Maximilians-University, Munich, Germany

## Supporting Information

**ABSTRACT:** Aggregation of the amyloid-forming  $\alpha$ -synuclein ( $\alpha$ S) protein is closely associated with the etiology of Parkinson's disease (PD), the most common motor neurodegenerative disorder. Many studies have shown that soluble aggregation intermediates of  $\alpha$ S, termed oligomers, permeabilize a variety of phospholipid membranes; thus, membrane disruption may represent a key pathogenic mechanism of  $\alpha$ S toxicity. Given the centrality of mitochondrial dysfunction in PD, we therefore probed the formation of ion-permeable pores by  $\alpha$ S oligomers in planar lipid bilayers reflecting the complex phospholipid composition of mitochondrial membranes. Using single-channel electrophysiology, we recorded distinct multilevel conductances (100–400 pS) with stepwise current transitions, typical of protein-bound nanopores, in mitochondrial-like membranes. Crucially, we observed that the presence of cardiolipin (CL), the signature phospholipid of mitochondrial membranes, enhanced  $\alpha$ S-lipid interaction and the membrane pore-forming activity of  $\alpha$ S oligomers. Further, preincubation of isolated mitochondria with a CL-specific dye protected against  $\alpha$ S oligomer-induced mitochondrial swelling and release of cytochrome *c*. Hence, we favor a scenario in which  $\alpha$ S oligomers directly porate a local lipid environment rich in CL, for instance outer mitochondrial contact sites or the inner mitochondrial membrane, to induce mitochondrial dysfunction. Pharmacological modulation of  $\alpha$ S pore complex formation might thus preserve mitochondrial membrane integrity and alleviate mitochondrial dysfunction in PD.

**KEYWORDS:**  $\alpha$ -Synuclein, oligomers, mitochondrial membrane, electrophysiology, pores, cardiolipin

### $\alpha$ -Synuclein nanopore



## INTRODUCTION

Parkinson's disease (PD) is the most common motor neurodegenerative disorder, with typical clinical signs including slowness of movement, muscular rigidity, resting tremor, and postural instability.<sup>1</sup> From a pathological perspective, it is classically associated with severe dopaminergic neuronal loss in the *substantia nigra*, with the defining presence of proteinaceous cytoplasmic inclusions in neuronal cell bodies and processes (known as Lewy bodies and Lewy neurites).<sup>2</sup> The major component of these deposits is an amyloid fibrillar form of the 14-kDa protein  $\alpha$ -synuclein ( $\alpha$ S), which is expressed abundantly in neurons and synapses. Many researches postulate that the generation of neurotoxic soluble intermediates, termed oligomers, along the aggregation pathway of  $\alpha$ S is central to the pathogenesis of PD.<sup>3,4</sup> Oligomeric aggregates of  $\alpha$ S have been consistently observed to disrupt a variety of membranes, in contrast to either native  $\alpha$ S

monomers or fibrils.<sup>5–7</sup> Downstream effects of membrane disruption may include dysregulation of cellular ionic homeostasis (especially  $\text{Ca}^{2+}$ ), altered signal transduction, free radical production, and activation of apoptosis, ultimately leading to synaptic degeneration and neuronal cell death.<sup>8–11</sup> Not least, the capacity of recombinant  $\alpha$ S oligomers to damage cellular membranes *in vitro* was found to correlate with *in vivo* dopaminergic neuron loss in the *substantia nigra* of rats expressing the same  $\alpha$ S variants.<sup>12,13</sup> A range of mechanisms for membrane permeabilization by  $\alpha$ S oligomers have been proposed, mainly: (i) membrane thinning (so-called “carpet-like” mechanism),<sup>14,15</sup> (ii) leakage provoked by the extraction of lipids (“detergent-like” mechanism),<sup>16–18</sup> and (iii) per-

Received: June 5, 2019

Accepted: July 29, 2019

Published: July 29, 2019

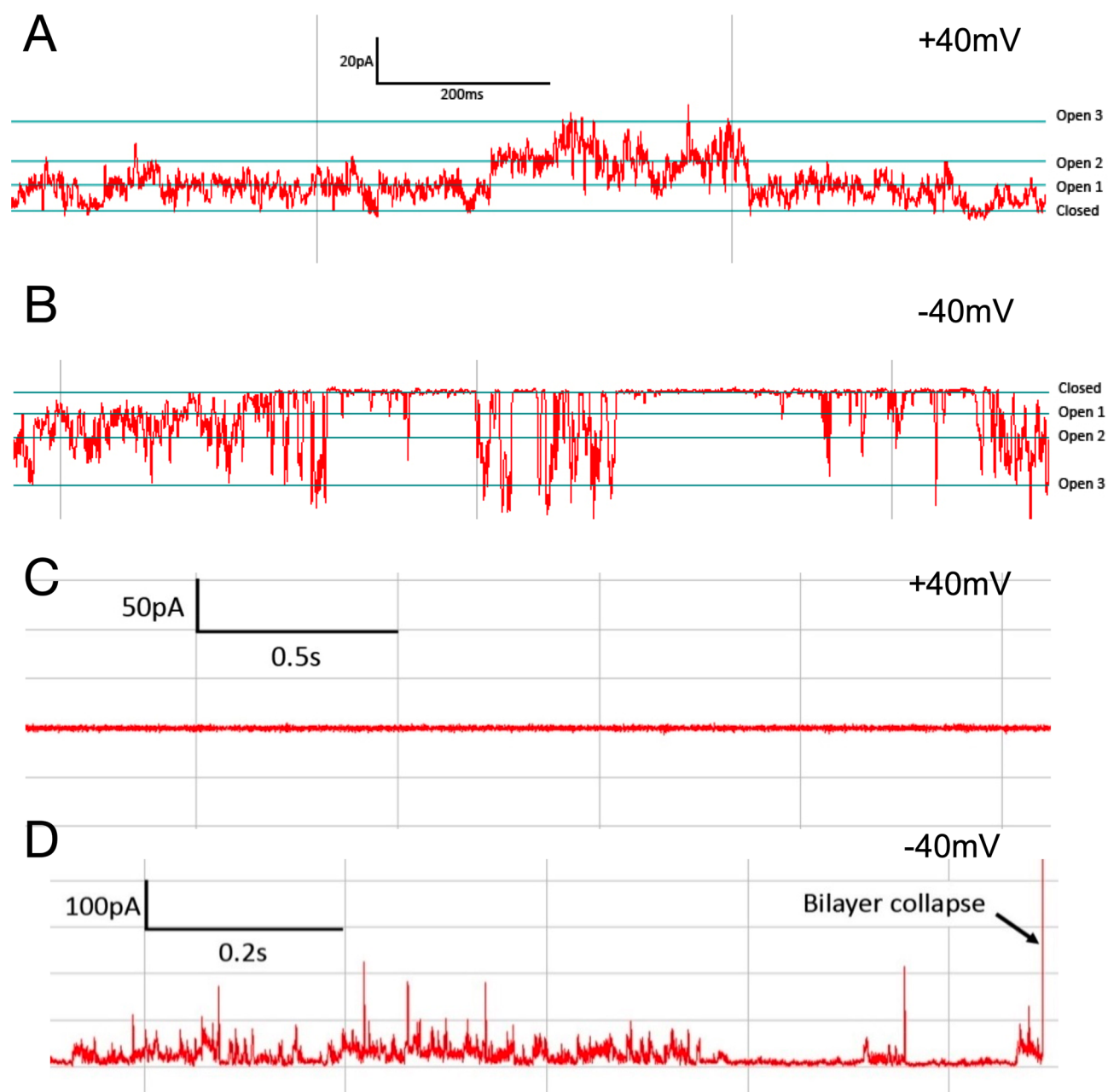


**Figure 1.** Single-channel current recordings induced by  $\alpha$ S oligomers in IM-type planar lipid bilayer. Planar lipid membrane recordings of  $\alpha$ S oligomers ( $1 \mu\text{M}$ ) in symmetrical KCl ( $250 \text{ mM}$ ) buffer on an IM-type ( $15\% \text{ CL}$ ) lipid bilayer, under voltage-clamp conditions of (A)  $+40 \text{ mV}$  and (B)  $-40 \text{ mV}$ . The current traces shown here, as represented by the electrical measurements, demonstrate “spiky” fast channel behavior; current fluctuations between three consecutive conductance levels (Open-1, Open-2, Open-3) can be resolved. (C) Example of a control trace obtained when monomeric  $\alpha$ S was added to the *cis*-chamber. (D) Bilayer collapse due to instability at high voltages ( $< -60 \text{ mV}$  or  $> +60 \text{ mV}$ ).

meabilization through pore formation (“poration” mechanism).<sup>19–21</sup> Regarding membrane poration, annular  $\alpha$ S oligomers with a central pore have been repeatedly reported and visualized using biophysical techniques such as atomic force microscopy (AFM),<sup>22</sup> cryo-electron microscopy (cryo-EM),<sup>23</sup> and small-angle X-ray scattering.<sup>24</sup> Computer modeling has also simulated the penetration of wild-type and mutant  $\alpha$ S in oligomeric ring-like conformations into membrane bilayers.<sup>25,26</sup>

The lipid composition of the phospholipid membrane and its attendant physical properties (e.g., membrane curvature, charge, and packing defects) play a major role in influencing  $\alpha$ S-membrane affinities.<sup>27,28</sup> In particular, oligomer–mem-

brane interactions are strongly favored by net negative charge and loose packing of the bilayer, which encourage electrostatic interactions with the positively charged N-terminus of  $\alpha$ S and hydrophobic (van der Waals) interactions with the acyl tails of membrane phospholipids, respectively, leading to membrane disruption.<sup>29–32</sup> A unique type of membrane is undoubtedly provided by energy-generating mitochondria organelles, which, like native  $\alpha$ S, populate axons and synapses to satisfy the high metabolic demand of dopaminergic neurons.<sup>33</sup> Mitochondria are surrounded by a complex double-membrane system, consisting of the outer (OMM) and inner (IMM) mitochondrial membranes, and mitochondrial contact sites, specialized domains formed in regions of close apposition between the

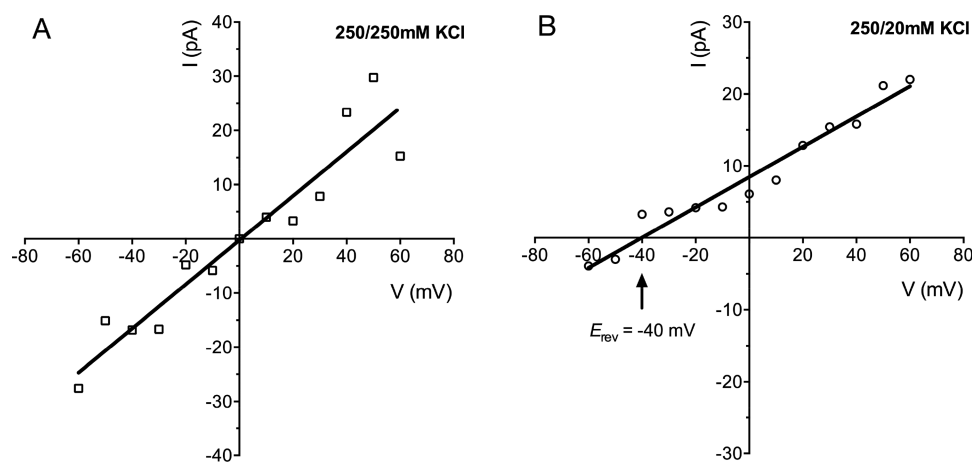


**Figure 2.**  $I/V$  curves of an  $\alpha$ S pore in IM-type bilayer. (A) Under symmetric (250/250 mM KCl, 10 mM MOPS/Tris, pH 7.2) conditions, the linear slope of the  $I/V$  graph is equivalent to the conductance  $G$  and corresponds to a single-channel conductance of 408 pS. (B) Under asymmetric conditions (250/20 mM KCl, 10 mM MOPS/Tris, pH 7.2), the intercept on the voltage axis for the  $I/V$  relationship corresponds to a reversal potential ( $E_{rev}$ ) at  $-40$  mV.

two membranes. The nonlamellar phospholipid cardiolipin (CL) constitutes 10–20% of mitochondrial membrane phospholipids and is enriched in the IMM and contact sites.<sup>34,35</sup> CL has an uncommon dimeric structure, resembling two phospholipids joined together via their headgroups. This gives CL a conical shape and a tendency to create high intrinsic curvature, as in the highly curved edges of mitochondrial membrane cristae.<sup>36</sup> Mitochondrial bioenergetic efficiency is dependent upon CL, since CL molecules stabilize supramolecular structures assembled from respiratory chain complexes in the IMM, thereby enhancing the facility of electron transfer and maximizing oxidative phosphorylation.<sup>37,38</sup> In point of fact, a decline in mitochondrial CL content was associated with bioenergetic deficits in mitochondria of neurons from  $\alpha$ -synuclein knockout mice.<sup>39</sup> It has been suggested that CL might help target oligomeric aggregates of  $\alpha$ S intracellularly to mitochondria and mediate disruption of mitochondrial membranes.<sup>40,41</sup> Mitochondrial imported  $\alpha$ S is predominantly associated with the CL-IMM, with the N-terminal segment of  $\alpha$ S being essential for its anchoring to mitochondria.<sup>42,43</sup> Compelling evidence has emerged from human dopaminergic neuronal cultures and post-mortem PD brains that  $\alpha$ S directly interacts with mitochondria, with potentially deleterious consequences.<sup>44,45</sup> However, the exact molecular mechanisms of  $\alpha$ S-induced mitochondrial dysfunction are still unclear.

Therefore, given the centrality of mitochondrial dysfunction in PD pathogenesis,<sup>46</sup> in the present study we sought to uncover whether  $\alpha$ S oligomers are able to permeabilize mitochondria membranes through ion-conducting pore formation and address whether this is connected to the presence of CL in the membrane. For this purpose, we make use of minimalist model systems consisting of freshly isolated mitochondria and single bilayer, or liposome, membranes that simulate the mitochondrial lipid environment.<sup>47</sup>

## RESULTS

A number of electrophysiological studies have previously shown that  $\alpha$ S can form oligomeric pores that exhibit channel-like properties in lipid membranes. Nevertheless, these studies have characteristically made use of one- or two-component bilayers that oversimplify the lipid complexity of biological

membranes.<sup>20,21,48</sup> Herein, we investigate the possible formation of conducting channels or pores by  $\alpha$ S in multicomponent bilayers that recapitulate the lipid constituents of the mitochondrial membrane. Native  $\alpha$ S (only monomeric) or aggregated  $\alpha$ S (an oligomer-enriched preparation) were applied separately, in physiologically relevant concentrations, to the mito-mimetic lipid bilayers. Formation of higher-order  $\alpha$ S oligomers in the aggregate preparation was confirmed using single-particle confocal analysis and immunoblotting characterization (Supporting Figure S1). Aggregation of  $\alpha$ S for generation of oligomers was performed using a well-established protocol involving ferric ions; these oligomers have already been extensively characterized by AFM and fluorescence correlation spectroscopy (FCS).<sup>49,50</sup> Moreover, they have been shown to alter intracellular calcium homeostasis and lead to cell death.<sup>51,52</sup>

**Electrophysiological Characterization of  $\alpha$ S Pores in Mito-Mimetic Lipid Bilayers.** In order to demonstrate and characterize the formation of ion-conducting  $\alpha$ S pores, the technique of planar bilayer membrane electrophysiology was used. The standard approach involves protein reconstitution into a BLM separating two electrolyte solutions. Since lipid membranes are almost perfect insulators, the formation of even a single conducting channel in a free-standing bilayer is detectable.<sup>53</sup> Uniquely, the bilayer was designed to have a phospholipid composition similar to that found in the IMM or mitochondrial contact sites (the latter representing regions of close apposition between the OMM and IMM), with a CL content of  $\sim 15\%$  (w/w) (IM-type: 45PC/25PE/10PI/SPS/15CL).<sup>34,54</sup> Recombinant Fe-induced  $\alpha$ S oligomers were added to the *cis*-side of an IM-type BLM at a final concentration of  $1 \mu\text{M}$ . At a clamped voltage of  $\pm 50$  mV and pH 7.2,  $\alpha$ S oligomers induced channel-like current events in the bilayer, an average of 35 min following addition of the  $\alpha$ S preparation into the electrolyte solution (range 7–100 min;  $n = 12$  trials with  $\alpha$ S oligomer preparation; refer to Supporting Table S2). Spontaneous membrane incorporation of  $\alpha$ S oligomers characteristically resulted in a sustained series of electrical bursts and spikes occurring on an otherwise current-free background, indicating fast, transient, and heterogeneous ionic events (Figure 1A,B). Importantly, channel-like activity was detected only in the presence of oligomeric but not

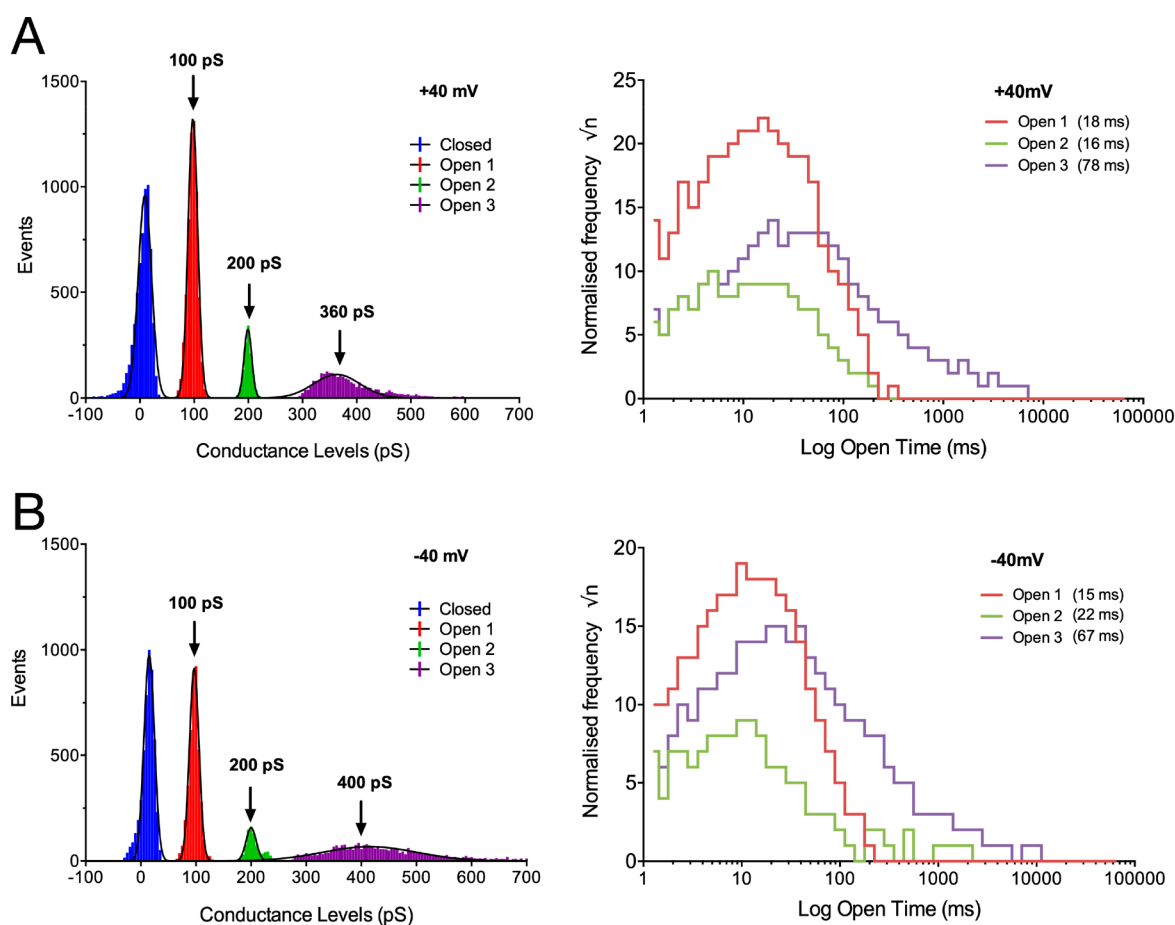


**Figure 3.** Histograms of multilevel conductance states and dwell-times of  $\alpha$ S pores in IM-type bilayers. Event histogram of closed and open conductance levels at (A, left panel) +40 mV and (B, left panel)  $-40$  mV holding potential, for  $\alpha$ S pore incorporated in IM-type bilayer. Data is fitted to Gaussian peaks (solid black lines). A first peak is assigned at 100 pS for a basic conductance event (Open-1), with subsequent peaks representing doubling of the conductances to 200 pS (Open-2) and subsequently 400 pS (Open-3). The minimum acceptable time interval for defining an open-state level was taken as 1 ms. The corresponding dwell-time histograms of the open states are shown for +40 mV (A, right panel) and  $-40$  mV (B, right panel). For optimal visualization of fit quality, dwell-times are accumulated into logarithmic bins and displayed with square-root ordinate.<sup>61</sup> The mean dwell-time (in ms) for each open state is given in brackets. Electrical recordings were carried out in 10 mM MOPS/Tris and 250 mM KCl at pH 7.2 and 23 °C.

monomeric  $\alpha$ S species ( $n = 10$  trials with  $\alpha$ S monomer preparations). Further, ion flux activity was never observed in bilayers without the addition of the protein ( $n = 10$  trials with DMSO/Fe aggregation buffer alone). A typical baseline current trace with monomer or buffer is shown in Figure 1C. Corresponding control experiments in which neither  $\alpha$ S monomer nor DMSO/Fe buffer led to any pore detections have been published previously.<sup>48</sup> Conductance across the membrane was measured upon applied voltages of  $\pm 40$  mV, since higher voltages considerably increased the instability of the bilayer and made recording unreliable (Figure 1D).

A detailed characterization of pore formation by the  $\alpha$ S aggregates in the IM-type bilayer was therefore undertaken, including information on current–voltage ( $I/V$ ) relationships, ion selectivity, a detailed analysis of conductance states, and estimation of pore size.  $I/V$  curves were constructed by plotting the amplitude of the current recorded at each clamped membrane potential ( $-60$  mV to  $+60$  mV) under symmetric (250/250 mM KCl) and asymmetric (250/20 mM KCl) conditions (Figure 2). Linear  $I/V$  relationships were observed in both situations, indicating that the rate of ion permeation through the  $\alpha$ S pore was not voltage-dependent. This possibly reflects a symmetrical distribution of electrical charges along

the pore axis. The mean conductance ( $G$ ) calculated from the straight-line fit of the graph was 408 pS (Figure 2A). Under asymmetrical conditions, an electrochemical diffusion gradient exists between the *cis*- and *trans*- compartments, due to buffers of different ionic concentrations. This allows the direction of shift in the reversal potential  $E_{\text{rev}}$  to be measured, and hence the cation or anion selectivity of a pore determined. Here, in asymmetric 250/20 mM KCl solutions at pH 7.2, the observed reversal potential corresponding to a zero current was  $E_{\text{rev}} = -40$  mV, indicating an anion-selective pore (Figure 2B).

Next, an analysis of all current traces was carried out to quantify multilevel conductance behavior, the latter being typical of the incorporation of channel-like pores. Indeed, well-defined conductance states were immediately apparent when a histogram of conductance levels (in pS) was constructed and the data fitted into Gaussian distribution. The Gaussian fits revealed distinct peaks at three conductance values, both at positive and negative applied holding potentials. At 40 mV, peaks occurred at  $\sim 100$  pS (Open-1),  $\sim 200$  pS (Open-2), and  $\sim 360$  pS (Open-3) (Figure 3A). At  $-40$  mV, peaks occurred at  $\sim 100$  pS (Open-1),  $\sim 200$  pS (Open-2), and  $\sim 400$  pS (Open-3) (Figure 3B). Furthermore, it was noted that the 3 conductance levels (Open-1, Open-2, and Open-3) appeared

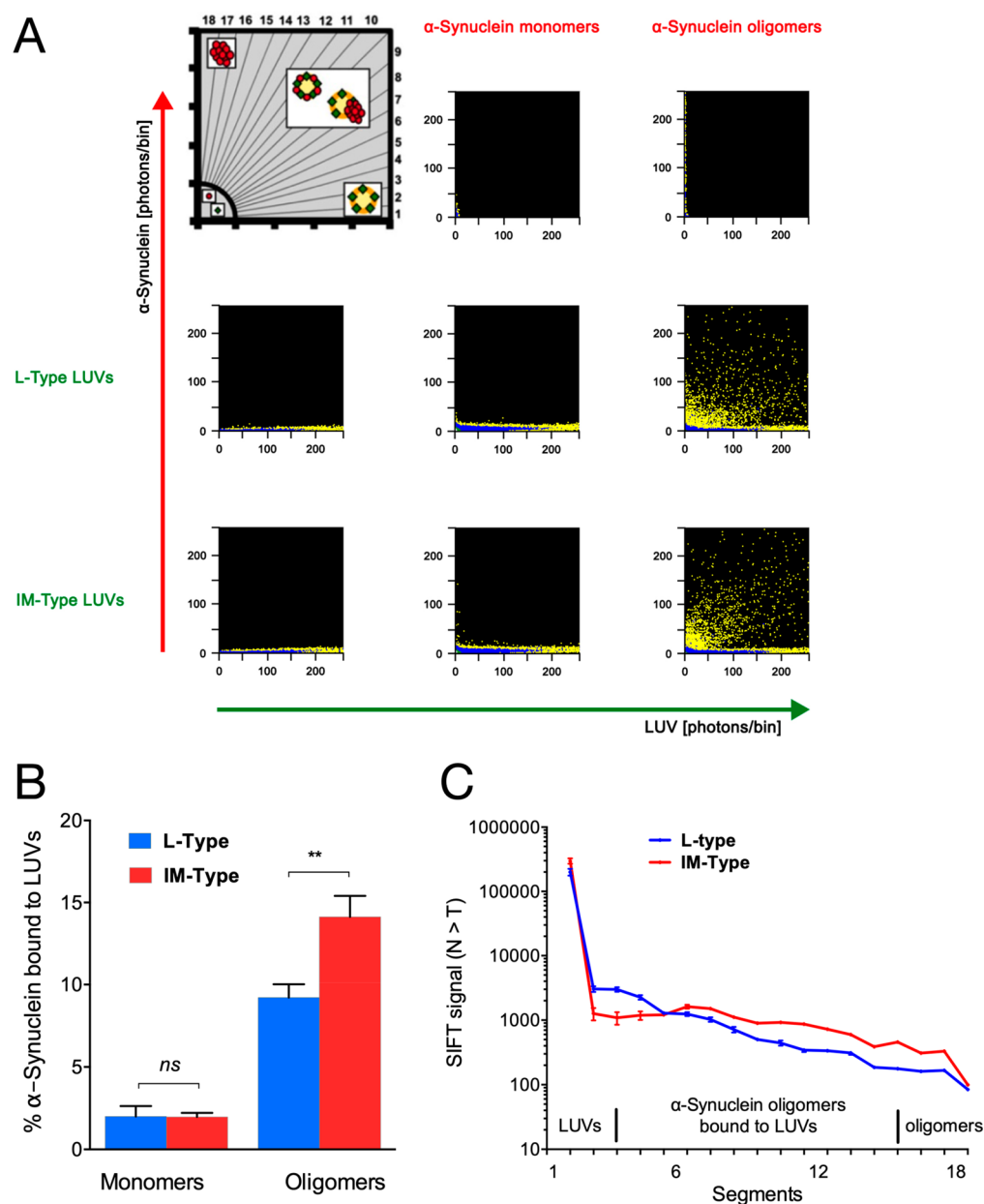


**Figure 4.** Confocal FCS analysis of  $\alpha$ S binding to mito-mimetic bilayers. (A) 2D-FIDA histograms depicting  $\alpha$ S monomers or aggregated oligomers and LUVs composed of either L-type (containing 0% CL) or IM-type (containing 15% CL) lipids. Thus, segments 1–3 correspond to the green-labeled LUVs alone; segments 4–15 correspond to bicolored particles indicating oligomers bound to LUVs; and segments 16–18 correspond to free red-labeled oligomers (refer to leftmost panel in the top row). Middle row panels from left to right: L-type vesicles without  $\alpha$ S, incubated with monomers, and incubated with Fe<sup>3+</sup>-induced oligomers. Bottom row panels from left to right: IM-type vesicles without  $\alpha$ S, incubated with monomers, and incubated with oligomers. *x*-axis, green fluorescence; *y*-axis, red fluorescence. Excitation at 488 and 633 nm. (B) Quantitative FIDA analysis of  $\alpha$ S bound to LUVs. For LUVs containing 15% CL (IM-type), the percentage of bound protein is significantly higher than for LUVs without CL (L-type). Values represent mean percentage  $\pm$  SEM ( $n = 5$ ). For statistical analysis, a paired *t*-test was used (ns:  $p > 0.05$ ; \*\*  $p < 0.01$ ). (C) SIFT segment analysis of  $\alpha$ S oligomers bound to LUVs. From segment 6 onward, a higher signal for bicolored particles is observed for IM-type LUVs than for L-type LUVs ( $n = 5$ ).

and disappeared sequentially, possibly indicating that structural arrangements within the same pore unit had occurred. Therefore, an analysis of the distribution of conductance steps was undertaken at +40 mV and –40 mV. The histograms of the conductance step size (Supporting Figure S3) lead to the identification of a major peak at  $\pm 90$ –100 pS, with subsequent lower peaks at  $\pm 180$ –200 pS and  $\pm 360$ –400 pS. The step sizes therefore overlapped with the conductance levels. Dwell-time graphs were also constructed to enable comparison of the duration (in ms) of the open states. The

dwell-time distributions and average lifetime values of the three open levels at +40 mV and –40 mV are shown in Figure 3A,B, respectively. The mean dwell-time values were similar for Open-1 and Open-2 levels ( $\sim 18$  ms) while the higher conductance state Open-3 had a significantly longer average lifetime ( $\sim 73$  ms).

Defined changes in conductance levels as described above imply the presence of protein-bound pores of  $\alpha$ S in IM-type bilayers. The pore diameter can be estimated from the conductance levels, assuming a simplified cylindrical nano-

pore<sup>21</sup> (see [Methods](#)). At applied voltages of +40 mV and -40 mV, the pore diameters were calculated for the three defined conductance values, yielding pore diameter estimates of 0.57 nm (Open-1, 100 pS), 0.82 nm (Open-2, 200 pS), and 1.18 nm (Open-3, 400 pS).

**Inhibition of Pore Insertion by Antiamyloid Compounds.** Since the electrophysiology experiments were indicating formation of nanosized pores or channels in IM-type bilayers by aggregated structures of  $\alpha$ S, we proceeded to attempt inhibition of membrane activity by testing antiaggregator compounds. We therefore tested the antioligomer compound anle138b, featuring a diphenyl-pyrazole scaffold which potently antagonizes  $\alpha$ S aggregation;<sup>55–57</sup> the natural flavonoid morin and BTE, both identified as lead inhibitors of  $\alpha$ S aggregation in previous work,<sup>58–60</sup> and ginkgolide B, a comparatively weak antiaggregator compound.<sup>58</sup> Prior to introduction into the test chamber, the preaggregated  $\alpha$ S preparation was incubated with the compounds for 90 min. The aggregate–compound mixture was then added to the *cis*-compartment and pore formation monitored over 2 h. Pore formation in IM-type lipid bilayers was completely absent when  $\alpha$ S oligomers had been mixed with 10  $\mu$ M anle138b ( $n = 0/6$  trials) or 10  $\mu$ M morin ( $n = 0/6$  trials; 0%). BTE at a concentration of 0.5  $\mu$ g/mL was marginally less effective in its inhibitory effect on pore formation ( $n = 1/6$  trials; 17%); the weakest inhibitor was 10  $\mu$ M ginkgolide B since the same multilevel conductance events typical of  $\alpha$ S pores in IM-bilayers were observed in a third ( $n = 2/6$  trials; 33%) of experiments. In summary, we demonstrated that use of antiaggregator molecules could effectively modulate the formation of membrane-active pores by  $\alpha$ S in mito-mimetic lipid bilayers.

**Pore Insertion Rate Is Dependent on CL Content of the Bilayer.** One of the aims of this work was to decipher how the lipid environment, especially CL, might affect the pore-forming ability of oligomeric  $\alpha$ S. Therefore, the rate of pore formation in IM-type bilayers was compared with that in two other bilayer types, namely L-type, which has the same phospholipid constituents as IM-type but lacks CL (60PC/25PE/10PI/5PS); and C-type, a phospholipid blend which reflects the composition of synaptic vesicle membranes (50PE/30PS/20PC)<sup>62</sup> and which has the same overall negative charge density (30% anionic) as IM-type membranes, thereby allowing us to control for an effect of anionic charge on  $\alpha$ S pore insertion. In all, 12 independent electrophysiology experiments were carried out with each bilayer type, thus ensuring collection of robust data. When  $\alpha$ S oligomers were added to the *cis*-chamber, channel-like membrane activity indicating formation of pores in the bilayer was reproducibly observed in 67% of trials with the IM-type bilayer ( $n = 8/12$  trials), 33% of trials with the L-type bilayer ( $n = 4/12$  trials) and 42% of trials with the C-type bilayer ( $n = 5/12$  trials). Crucially, no pores were detected during blank runs using aggregation buffer only, in the absence of  $\alpha$ S ( $n \geq 3$  trials for each lipid bilayer type). We also looked at the time that elapsed before incorporation of the first pore in the bilayer, for each positive trial. No statistically significant differences were observed in the mean (36, 32, 34 min), the median (27, 16, 10 min), the minimum (8, 11, 7 min), or the maximum (100, 85, 95 min) time to first opening when comparing IM-type, L-type, and C-type bilayers, respectively (refer to [Supporting Table S2](#) for full details). Taken together, our data is suggestive of a preference for  $\alpha$ S oligomers to act as pore-forming agents

in bilayers recapitulating the complex lipid constituents of mitochondrial membranes with a high CL content (IM-type).

**Analysis of  $\alpha$ S-Membrane Binding Using FCS.** The influence of CL on the interaction between  $\alpha$ S oligomers and lipid bilayers was explored in greater detail using confocal fluorescence correlation spectroscopy. FCS allows quantification of the binding of peptides and proteins to phospholipid vesicles, using nanomolar protein concentrations. Further, aggregate formation can be monitored with high sensitivity by SIFT analysis.<sup>63–65</sup> To evaluate  $\alpha$ S aggregation and lipid binding, 10–20 nM Alexa-647  $\alpha$ S (red label), either in monomeric form or aggregated into oligomers, was mixed with 100 nm LUVs loaded with Alexa-488 dye (green label). Histograms using 2D-FIDA were constructed from SIFT measurements of  $\alpha$ S coincubated with IM-type (15% CL) or L-type (0%CL) LUVs ([Figure 4A](#)). For  $\alpha$ S monomers, high-intensity bins were observed only along the *x*-axis of the histograms (“purely green bins”). These bins are generated by LUVs alone, devoid of bound  $\alpha$ S. Therefore, there was practically no interaction between monomeric  $\alpha$ S and IM-type or L-type membranes ([Figure 4A](#), middle column panels). Aggregates representing Alexa-647  $\alpha$ S oligomers were observed as an accumulation of high intensity bins along the *y*-axis (“purely red bins”) ([Figure 4A](#), top-right panel). When mixed with either IM-type or L-type LUVs, these  $\alpha$ S oligomers yielded bins with both green and red fluorescence, indicating that the oligomers had mostly associated with the vesicles. Further, in the presence of LUVs, fewer purely red bins with high fluorescent intensity (i.e., free oligomers) could be detected ([Figure 4A](#), right column panels). The exact fraction of bound  $\alpha$ S to IM-type and L-type vesicles was calculated by a 2D-FIDA fit ([Figure 4B](#)). A higher amount of bound protein was observed for oligomer samples in comparison to monomer samples for both IM-type and L-type membranes (monomers: < 5% bound). More pertinently, FIDA analysis demonstrated that  $\alpha$ S oligomers exhibited a modest increase in propensity to bind IM-type membranes in LUVs compared to binding observed for L-type vesicles, which was statistically significant (IM-type: 14.1%, L-type: 9.2%;  $p = 0.009$ ). This can also be seen in the 2D-FIDA segment analysis ([Figure 4C](#); refer to [Supporting Figure S4](#) for explanation of 2D-FIDA histogram segments) where from segment 6 onward, a higher signal for bicolored particles, indicating bound oligomers, was observed for LUVs containing 15% CL (IM-type) than for LUVs without CL (L-type) ( $p = 0.0144$ ). Hence, in line with our previous findings, the  $\alpha$ S oligomers manifested a moderate, albeit higher, affinity for LUVs specifically containing the mitochondrial lipid cardiolipin.

**Targeting CL Inhibits  $\alpha$ S-Induced Swelling and Cyto c Release from Isolated Mitochondria.** The induction of pores in mitochondrial membranes would be expected to lead to membrane permeabilization and dysfunctional events, such as organelle swelling and the release of apoptogenic cytochrome *c* (cyto *c*) from mitochondria.<sup>66,67</sup> Hence, we took a further step to investigate the possible consequences on isolated mitochondria of exposure to the Fe<sup>3+</sup>-induced  $\alpha$ S oligomers. We observed a dose-dependent effect at low micromolar oligomer concentrations on mitochondrial swelling ([Figure 5A,B](#)): end-point (i.e., at  $t = 30$  min) swelling by 1–2  $\mu$ M  $\alpha$ S oligomers was ~50% of the effect of Ca<sup>2+</sup> ions, with a more pronounced degree of swelling at 3  $\mu$ M ( $76 \pm 5.8\%$ ). In contrast, 2  $\mu$ M monomeric (i.e., fresh)  $\alpha$ S did not lead to any significant swelling above control ( $25 \pm 0.5\%$ ; 2  $\mu$ M  $\alpha$ S-fresh

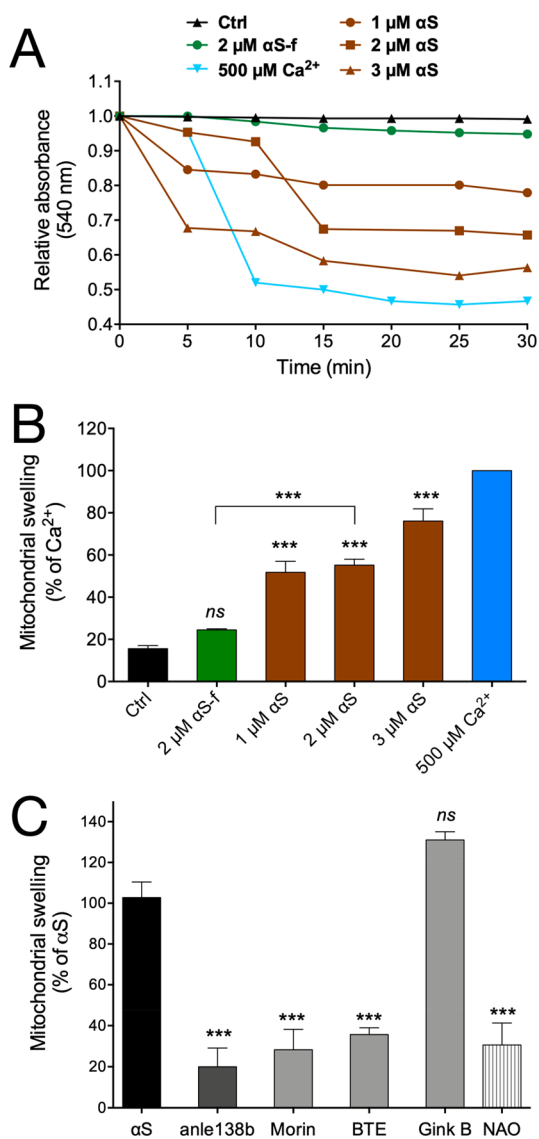


**Figure 5.** Mitochondrial swelling by  $\alpha\text{S}$ . (A) Swelling kinetics of freshly isolated mitochondria exposed to 1–3  $\mu\text{M}$  aggregated  $\alpha\text{S}$  ( $\alpha\text{S}$ ), 2  $\mu\text{M}$  fresh  $\alpha\text{S}$  ( $\alpha\text{S-f}$ ), or 500  $\mu\text{M}$   $\text{Ca}^{2+}$  (positive control). Mitochondrial swelling was measured by monitoring the absorbance at 540 nm for 30 min, and typical traces are shown. (B) Maximal swelling of mitochondria after 30 min exposure to  $\alpha\text{S}$  was calculated as a percentage of  $\text{Ca}^{2+}$ -induced swelling.  $\alpha\text{S}$  concentrations are in moles of monomeric  $\alpha\text{S}$ . Values represent the means  $\pm$  SEM ( $n = 3-6$ ); one-way ANOVA for multiple comparisons with control or between the marked pairs; \*  $p < 0.05$ , \*\*\*  $p < 0.001$ , ns, nonsignificant difference ( $p > 0.05$ ). (C) The antioligomer compound anle138b, the polyphenols morin and ginkgolide B (all at 10  $\mu\text{M}$ ), and black tea extract (BTE; 0.5  $\mu\text{g}/\text{mL}$ ) were preincubated separately with mitochondria before  $\alpha\text{S}$  oligomers (2  $\mu\text{M}$ ) were added. Mitochondrial swelling in the presence of each compound after 30 min is given as a percentage of the  $\alpha\text{S}$  control (100%). Values represent means  $\pm$  SEM ( $n = 2-4$ ); \*\*\*  $p < 0.001$  and ns, nonsignificant difference, compared with control (one-way ANOVA with Bonferroni's post hoc analysis).

vs 2  $\mu\text{M}$   $\alpha\text{S}$ -oligomers,  $p = 0.0002$ ). The same group of compounds that we had previously tested against  $\alpha\text{S}$  pore formation were now assayed for their ability to prevent mitochondrial swelling (Figure 5C). Interestingly, a similar pattern of inhibition to the electrophysiology experiments was

noted, with anle138b being the strongest and ginkgolide B the weakest inhibitor of  $\alpha\text{S}$ -induced swelling: anle138b ( $20 \pm 9\%$ ,  $p < 0.0001$ ) > morin ( $28 \pm 10\%$ ,  $p = 0.0002$ ) > BTE ( $36 \pm 3\%$ ,  $p = 0.0007$ ) > ginkgolide B ( $131 \pm 4\%$ ,  $p > 0.05$ ). The inference is that the active compounds were acting with similar, antioligomer-based mechanisms. We also considered the potential involvement of mitochondrial permeability transition pore (mPTP) opening in mitochondrial swelling by  $\alpha\text{S}$  oligomers. However, none of the classical pharmacological modulators of mPTP manifested any significant inhibitory effect on swelling; these included the voltage-dependent anion channel (VDAC) inhibitor DIDS (108%), monoclonal antibodies to VDAC (127%), the adenine nucleotide translocator (ANT) inhibitor BKA (125%), and the strong antioxidant *N*-acetylcysteine (102%). Given that the electrophysiology and FCS experiments had suggested a major influence of CL on  $\alpha\text{S}$ -induced poration of mitochondrial-like membranes, we proceeded to test this hypothesis in the swelling assay too. Hence, isolated mitochondria were first incubated with a molecular probe which has a strong and specific binding affinity to CL, namely 10-*N*-nonyl acridine orange (NAO).<sup>68,69</sup> Indeed, NAO dramatically decreased swelling induced by  $\alpha\text{S}$  oligomers ( $31 \pm 5\%$ ,  $p < 0.0001$ ) (Figure 5C).

Another classical readout for mitochondrial membrane permeabilization is the mobilization and efflux of cyto *c* from stores within the intermembrane space and IMM.<sup>70,71</sup> Thus, isolated mitochondria were exposed to 2  $\mu\text{M}$   $\alpha\text{S}$  oligomers and the amount of cyto *c* release (CCR) from mitochondria determined by immunoblotting of the recovered supernatant (Figure 6A). Semiquantitative densitometric analysis of the

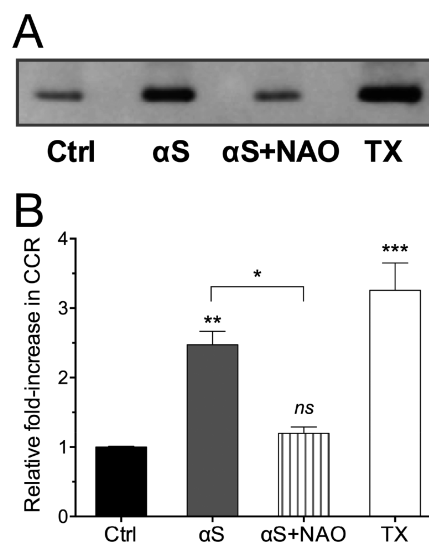


**Figure 6.** Immunoblotting and densitometry of CCR by  $\alpha\text{S}$ . (A) Cyto *c* released from isolated mitochondria incubated with  $\alpha\text{S}$  oligomers (2  $\mu\text{M}$ ,  $\alpha\text{S}$ ) alone or in the presence of NAO (20  $\mu\text{M}$ ,  $\alpha\text{S+NAO}$ ) and with 5% Triton X-100 (TX) was visualized by immunoblot analysis of the supernatant probed with anticyclochrome *c* antibody. Control (Ctrl) represents “background” cyto *c* released into the supernatant from untreated mitochondria in buffer alone. Bands from a representative gel are shown ( $n = 2$ ). (B) Blots were analyzed by densitometry, illustrating fold-increase in CCR compared to control. Values represent means  $\pm$  SEM ( $n = 2$ ); \*  $p < 0.05$ , \*\*  $p < 0.01$ , \*\*\*  $p < 0.001$ , ns, nonsignificant difference (one-way ANOVA relative to Ctrl or between indicated pairs).

resultant cyt *c* bands (Figure 6B) showed a robust  $\sim 2.5$ -fold increase in CCR over control mitochondria ( $p < 0.01$  vs control) and around 75% of the maximal effect of the detergent Triton X-100 (3.3-fold increase). Remarkably, when the CL-specific probe NAO was preincubated with mitochondria, the increase was only 1.2-fold and not significantly different from control mitochondria alone. Hence, both the swelling and CCR results strengthen the notion that membrane CL plays an important part in mediating mitochondrial toxicity by  $\alpha S$  oligomers.

**Assay for Interaction of CL with  $\alpha S$  Oligomers in Solution.** The high affinity of NAO for CL can be put to use in an assay to determine whether  $\alpha S$  protein can bind free CL phospholipids in solution. The underlying assay principle is that when NAO binds CL there is a decrease in NAO emitted fluorescence at 525 nm, as a result of dimerization of the dye molecules which brings them in close proximity to each other.<sup>72,73</sup> Thus, it would be expected that if  $\alpha S$  oligomers competitively bind CL, NAO would remain in monomeric form and no decrease in fluorescence would be observed. In fact, NAO fluorescence emission intensity at 525 nm decreased from 1.0 RFU (normalized value for NAO alone) to  $0.256 \pm 0.03$  RFU with addition of CL, but not upon mixing with PC ( $1.27 \pm 0.11$  RFU) or PS ( $1.15 \pm 0.06$  RFU). This confirms specificity of the assay to detect NAO-CL binding. However, preincubation of CL with  $\alpha S$  oligomers did not effectively prevent NAO dimerization ( $0.275 \pm 0.01$  RFU) (Figure 7). Hence, evidence for a direct CL- $\alpha S$  binding in solution could not be obtained using this assay.

## DISCUSSION

The interaction of soluble  $\alpha S$  oligomers with mitochondria is thought to induce mitochondrial dysfunction and contribute to early dopaminergic neuronal death in PD.<sup>74–76</sup> However, whether this interaction can lead to mitochondrial membrane

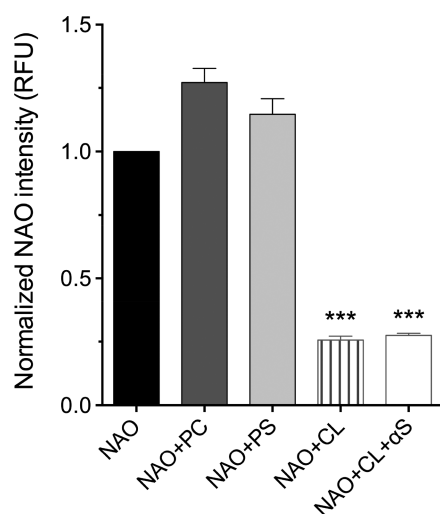


**Figure 7.** NAO-CL fluorescence binding assay. As expected, incubation of  $2 \mu\text{M}$  CL with NAO resulted in a highly significant decrease in NAO fluorescence emission at 525 nm, while neither the zwitterionic PC nor anionic PS had any effect, confirming NAO-CL affinity. Preincubation of CL with  $2 \mu\text{M}$   $\alpha S$  oligomeric species did not alter NAO-CL binding either. Fluorescence values are normalized to NAO alone (1.0) and represent means  $\pm$  SEM ( $n = 3$ ); \*\*\*  $p < 0.001$ , relative to NAO control (one-way ANOVA for multiple comparisons).

poration and the role of the local lipid environment had not been reported until the present study. In this work, we make use of single-channel electrophysiology to demonstrate the membrane pore-forming activity of  $\alpha S$  oligomers in membranes made up of a physiological lipid composition that simulates the mitochondrial environment (IM-type). We also reveal that the presence of CL, the signature phospholipid of mitochondrial membranes, promotes the formation of such pores and is crucial for mitochondrial permeabilization resulting in organelle swelling and loss of cyt *c*.

Conductance state and step-size histograms obtained from the electrophysiology experiments of  $\alpha S$  oligomers in IM-type membranes show clear peaks at the same conductances, i.e., 100, 200, and 400 pS. Published literature reporting on channel formation by  $\alpha S$  in negatively charged BLM (however with bilayers consisting of only one or two different phospholipids) also typically documented major conductance states also in the hundreds of pS.<sup>19–21,77</sup> Therefore, the histograms strongly suggest the formation of holes spanning the bilayer that are surrounded and stabilized by  $\alpha S$  oligomeric assemblies. Less likely is the possibility of toroidal lipidic pore formation, as a result of protein clustering on the membrane surface, which would fluctuate continuously in size and hence not explain the consistency of the conductance levels and step sizes observed here.<sup>78</sup> Also unlikely is a “carpeting” effect of the  $\alpha S$  aggregates on the outer leaflet of the membrane with thinning of the membrane, facilitating leakage of ions across the bilayer—in the case, defined steps in current would be absent, too.<sup>79,80</sup>

The observation from the conductance state histograms that  $G_{\text{Open } 2}$  (200 pS) is twice that of  $G_{\text{Open } 1}$  (100 pS), and that  $G_{\text{Open } 3}$  (400 pS) is in turn twice that of  $G_{\text{Open } 2}$ , suggests that three types of pores may be interconverting with each other in the membrane. Keeping in mind the idea of loosely interacting mobile protein subunits in a fluidic bilayer,<sup>81</sup> a number of scenarios can be envisaged. First, is the presence of a single pore in the bilayer which changes the pore dimensions reflecting the association or disassociation of a fixed subunit (Figure 8A). Thus, starting for example from a minimal Open-1 (100 pS) pentameric pore (0.57 nm pore diameter) incorporated into the bilayer, addition of a single  $\alpha S$  subunit results in assembly of a hexameric Open-2 (200 pS) pore (Open-1  $\rightarrow$  Open-2), which in turn may associate with another  $\alpha S$  subunit to generate an Open-3 (400 pS) heptameric pore (Open-2  $\rightarrow$  Open-3). Closure of either of the three types of pores into a nonconducting (closed) state would generate conductance steps of 100, 200, and 400 pS for Open-1 (Open-1  $\rightarrow$  Closed), Open-2 (Open-2  $\rightarrow$  Closed), and Open-3 (Open-3  $\rightarrow$  Closed), respectively. Further, longer dwell-times and a broader conductance distribution observed for Open-3 pores would be in keeping with a greater degree of heterogeneity in pore size diameter permissible as a result of the assembly from a greater number of loosely interacting mobile protein subunits in the fluidic bilayer. A second possibility is that the 100 pS (Open-1), 200 pS (Open-2), 400 pS (Open-3) pores reflect coupled multimeric assemblies that have 1, 2, or 4 pores of the same size in a mono-, di-, or tetrameric supermolecular structure (Figure 8B). Again, this would explain the defined 100, 200, and 400 pS jumps, as well as the longer dwell-times of Open-3 pores (a more stable tetrameric complex). A third possible model would involve the formation of up to four identical and separate pores, each with a 100 pS (Open-1) conductance. However, a distinct

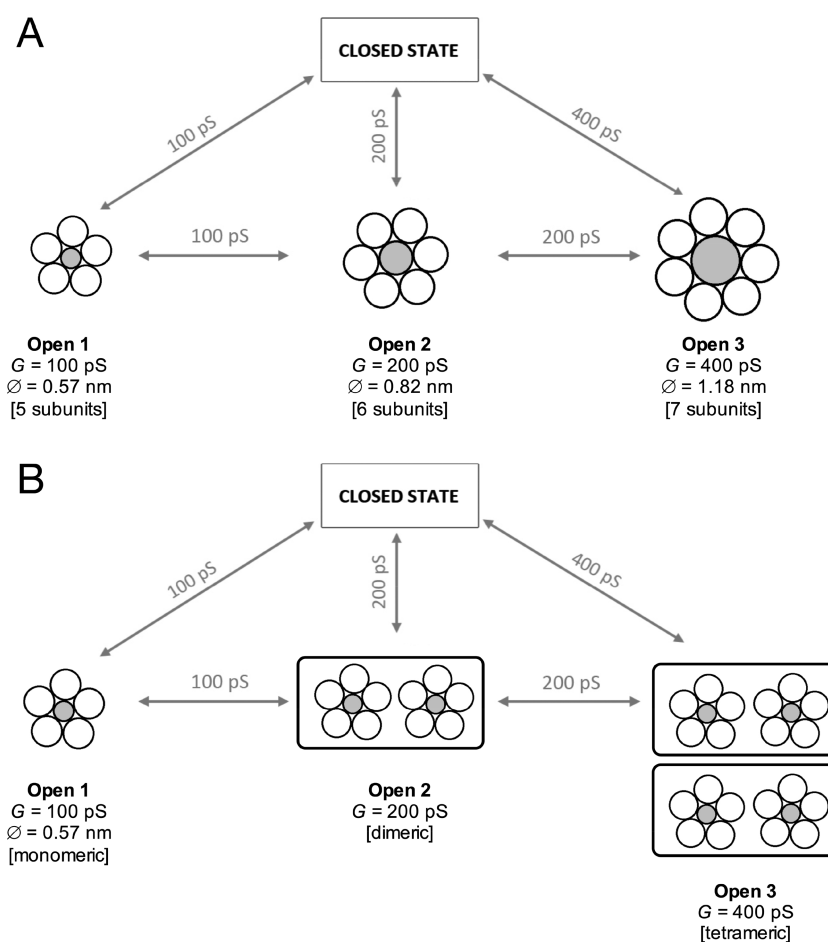


**Figure 8.** Schematic models accounting for the multiple conductance states generated by  $\alpha$ S oligomers in IM-type bilayers. (A) Open-1 (100 pS), Open-2 (200 pS), and Open-3 (400 pS) conductance ( $G$ ) levels can be explained by assuming incorporation, or release, of a fixed subunit into an existing  $\alpha$ S multimeric aggregate complex with a ring-like structure. The pore lumens are represented by the central gray circles with increasing radii. Pore diameters ( $\varnothing$ ) are drawn to scale in relation to each other. (B) Open-1 (100 pS), Open-2 (200 pS), and Open-3 (400 pS) conductance ( $G$ ) levels reflect the formation of coupled multimeric assemblies that have 1, 2, or 4 pores of the same size in a mono-, di-, or tetrameric supramolecular structure. Defined subunits constituting the pore assemblies are represented by white circles. Conductance steps between open and closed states are shown as bidirectional arrows (in pS).

conductance level or step size at  $\sim 300$  pS (i.e., reflecting the simultaneous opening/closure of three Open-1-sized pores) is notably absent from the histograms (Figure 3 and Supporting Figure S3), thereby mitigating against the latter scenario.

Analogous channel models to those illustrated in Figure 8 have already been described. For instance, molecular dynamics (MD) simulations of docking of  $\alpha$ S molecules onto membranes show “propagating docking” by incorporation of  $\alpha$ S monomers in lipid membranes to form energetically favorable pentamers and hexamers,<sup>82</sup> while Tosatto and co-workers hypothesized that insertion or removal of a tetrameric  $\alpha$ S subunit to a single pore accounted for transitions between the observed multilevel channel conductances of  $\alpha$ S channels in simple binary planar membranes.<sup>21</sup> It is also useful to compare the electrophysiological features of Fe-induced  $\alpha$ S oligomers in IM-type bilayers with those reported in previous work using azolectin (PC) bilayers. Similarities include bilayer conductances of 100–600 pS, voltage-independence, and a preference for permeability to negatively charged ions such as chloride ions ( $P_{\text{Cl}^-}/P_{\text{K}^+} \cong 2.75$ ).<sup>48,49</sup> Impressively, pore-like structures were actually visualized on AFM after incubation of isolated mitochondria with recombinant N-terminus of human  $\alpha$ S (amino acid residues 1–60), which was associated with

mitochondrial swelling.<sup>83</sup> The exact nature of the  $\alpha$ S oligomeric pore(s) in the IM-type membrane observed here, however, remains to be determined in future studies, for example by applying single-molecule optical detection using fluorescently labeled peptides in a horizontal bilayer system.<sup>84</sup>

What are the potential pathophysiological sequelae of punching nanometer-sized holes in mitochondria? Here, we observed that  $\alpha$ S oligomers (but not monomers) led to significant mPTP-independent swelling and CCR from isolated mitochondria. Moreover, in our previous work, fibrillary  $\alpha$ S was not found to significantly permeabilize mito-mimetic liposomes<sup>40</sup> or form pores in planar lipid bilayers.<sup>48</sup> In close accordance with these findings, it was reported that soluble  $\alpha$ S oligomers, but not monomeric or fibrillary  $\alpha$ S, added exogenously to mitochondria induced organelle swelling, depolarization, and CCR, which were only partially rescued by inhibition of the mPTP.<sup>85</sup> Intriguingly, there are several examples of virulent toxins from bacterial pathogens that specifically target and disrupt mitochondrial membranes. For example, the p58 subunit of *Helicobacter pylori* VacA toxin forms hexameric or heptameric oligomeric pores in mitochondrial membranes with a low but significant conductivity of 12 pS (calculated diameter of 0.15 nm) and having a clear

preference for anions.<sup>86</sup> Another bacterial porin, *Neisseria gonorrhoeae* PorB, incorporates into the IMM with a main conductance state of ~420 pS; it was calculated that a single open such channel would dissipate the mitochondrial membrane potential in about 0.8 ms.<sup>87</sup> Hence, mechanistically, amyloid  $\alpha$ S pores in mitochondrial membranes might be acting analogous to bacterial mitochondrial porins.

Another important question addressed in this investigation was how much a change in lipid composition, in particular the presence of CL, affects the membrane pore-forming activity of  $\alpha$ S. Collective evidence is obtained here invoking the necessity of an interaction of  $\alpha$ S oligomers with CL for perturbation of mitochondrial integrity: (i) successful membrane incorporation for  $\alpha$ S was most frequently observed in bilayers that recapitulate the properties of the inner mitochondrial membrane and contact sites; (ii)  $\alpha$ S oligomers had a significantly lower affinity for binding to vesicles lacking membrane CL; (iii) pretreatment of mitochondria with a CL-specific probe (NAO) dramatically reduced mitochondrial swelling and offered protection against CCR. The fact that NAO is specific for CL is based on considerable research<sup>68,88–90</sup> and was confirmed here in the CL-NAO fluorescence binding experiments. Our data is in agreement with several recent reports highlighting the interaction of  $\alpha$ S with CL in mitochondrial membranes. Thus,  $\alpha$ S interacted strongly with, and fragmented, lipid vesicles whose composition matched that of the CL-containing IMM.<sup>91,92</sup> Mitochondrial studies have shown that  $\alpha$ S binds significantly to the IMM membrane but not to the OMM, which contains less CL;<sup>42</sup> however, with an increase of CL phospholipid in the OMM, clusters of  $\alpha$ S protein accumulate at the mitochondrial surface and mitochondria display fragmentation.<sup>93</sup> The propensity for  $\alpha$ S-CL interaction may be partly explained by way of electrostatic attractions between the divalent anionic charge from the diphosphatidyl glycerol headgroup of CL and the positively charged lysine residues in the N-terminal repeat domain of  $\alpha$ S. Yet, the pore insertion rate of  $\alpha$ S oligomers was reduced by half (from 67% to 33%) when changing from IM-type to C-type lipid BLMs—even though both membrane types possess the same overall negative charge. Hence, an additional important factor is likely the affinity of  $\alpha$ S for lipid packing defects, typically found in membranes harboring cone-shaped lipids like CL which induce negative curvature strain.<sup>15,36</sup> Such defects would facilitate insertion of  $\alpha$ S oligomers into the headgroup region. The fact that we failed to demonstrate a direct binding between CL and  $\alpha$ S oligomers in solution, lends more support to an interaction with CL at mitochondrial membrane surfaces *in situ*, by way of curvature and packing defects. Strikingly, the endogenous mitochondrial porins Bax and Bak also insert within curvature-induced lipid packing defects created by CL, leading to mitochondrial outer membrane permeabilization and triggering of apoptosis.<sup>94</sup> CL also guides the entry of cobra venom cytotoxins into mitochondrial membranes, leading to membrane poration and disruption of mitochondrial integrity.<sup>95</sup> It is surely fascinating that, once again, the molecular mechanism of pore insertion into mitochondrial membranes uncovered here for amyloidogenic  $\alpha$ S peptides, may be shared by natural cytotoxins.

Finally, we demonstrated that protection of mitochondria from poration and swelling can be accomplished by preincubation of  $\alpha$ S with strong (anle138b, morin and BTE) but not weak (GinkB) antiaggregator compounds.<sup>58</sup> Sufficient

time was allowed for compound interaction with  $\alpha$ S prior to insertion into the membrane, and all the three effective compounds are known to have direct modulatory effects on the aggregation pathway of  $\alpha$ S.<sup>55,59,60</sup> Moreover, anle138b blocked pore-like ionic current activity of channels formed by amyloid-beta ( $A\beta$ ) oligomers.<sup>96</sup> Thus, we conjecture that compound-oligomer interaction is the dominant mechanism involved, even though we cannot exclude concomitant compound-membrane effects.

The exciting possibility is raised that small-molecule compounds that modulate formation of amyloid  $\alpha$ S nanopores in mitochondrial bilayers may be considered as candidate drugs in the ongoing search for mechanism-based, rational therapeutics for PD.

## CONCLUSIONS

In conclusion, our data provide evidence of the molecular mechanisms by which soluble  $\alpha$ S aggregation intermediates may contribute to mitotoxicity in Parkinson's disease. We showed, for the first time, that ion-permeable pore structures are formed by  $\alpha$ S oligomers in mito-mimetic membranes. The  $\alpha$ S pores display features of amyloid peptide channels, including heterogeneous multilevel conductances in the order of 100s of pS, voltage-independence, and inhibition of membrane poration by antiaggregator compounds like anle138b. We conclude that the pores would be large enough to let water, ions (e.g., chloride ions), or small molecules transit through the bilayer, thus explaining the observed oligomer-induced swelling of, and release of cyto *c* from, isolated mitochondria. Outer mitochondrial contact sites or the IMM present a lipid environment containing high CL, which favors the membrane-pore forming activity of  $\alpha$ S. Future work should aim at intervening on the  $\alpha$ S-CL interaction, to prevent active  $\alpha$ S-induced pores in mitochondrial membranes and alleviate mitochondrial dysfunction in PD.

## METHODS

**Materials.** Bongkrecic acid (BKA) and anti-VDAC antibody were purchased from Calbiochem (EMD Chemicals Inc., Darmstadt, Germany). 10-N-Nonyl acridine orange (NAO) was purchased from Invitrogen (Thermo Fisher Scientific, U.S.A.). The phospholipids L- $\alpha$ -phosphatidylcholine (egg PC), L- $\alpha$ -phosphatidylethanolamine (egg PE), L- $\alpha$ -phosphatidylinositol (soy PI), L- $\alpha$ -phosphatidylserine (brain PS), DOPE:DOPS:DOPC (5:3:2 w/w/w), and heart cardiolipin were obtained from Avanti Polar Lipids, Inc. (Alabaster, AL, U.S.A.). All other chemicals, including the compounds morin, black tea extract (BTE; > 80% theaflavins), and ginkgolide B, were purchased from Sigma-Aldrich (Munich, Germany).

**Preparation of  $\alpha$ S Oligomers.** Recombinant  $\alpha$ S protein was expressed from a bacterial plasmid (pET-5a) containing full-length wild-type  $\alpha$ S in BL21(DE3) *E. coli* cells and purified as previously described in Nuscher et al.<sup>97</sup> Protein stock solutions of 1 mg/mL were prepared in 50 mM Tris-HCl (pH 7.0) buffer and stored at  $-80$  °C; to avoid repeated freeze/thawing, samples were divided into aliquots in LoBind tubes (Eppendorf). Oligomers of  $\alpha$ S were prepared using an established protocol,<sup>48</sup> by incubation with organic solvent and ferric ions: monomeric  $\alpha$ S (7  $\mu$ M) was incubated for 72 h in 50 mM Tris-HCl (pH 7.0) with 1% dimethyl sulfoxide (DMSO) and 20  $\mu$ M FeCl<sub>3</sub> without agitation at 25 °C in a total volume of 200  $\mu$ L.

**Planar Lipid Bilayer Electrophysiology Recordings.** Electrophysiological studies were carried out using an Ionovation Compact automated bilayer workstation (Ionovation GmbH, Osnabrück, Germany) on an isolated vibration-free table. Ag/AgCl electrodes (Ionovation GmbH) with 2 M KCl/agarose bridges (1.5% w/v agarose) were used to apply the transmembrane voltage and to

measure the transmembrane current. The *cis*-electrode was connected to the headstage of a HEKA EPC10 amplifier (HEKA Elektronik GmbH) and used as a reference for the reported current readings.

All aqueous solutions used for electrophysiology were prepared using doubly distilled and deionized water, filtered through a 0.4- $\mu\text{m}$  filter, and stored at 4 °C. Lipid mixtures for the bilayer membrane were prepared by mixing lipid solutions in chloroform in the defined ratios (IM-type: 45PC/25PE/10PI/SPS/15CL; L-type: 60PC/25PE/10PI/SPS; or C-type, 50PE/30PS/20PC) and then drying under vacuum. The dried lipid mixture was redissolved in *n*-decane to obtain a concentration of 30 mg/mL. This phospholipid solution was added to the chamber and used to form a vertical bilayer membrane (BLM) by spreading the lipid up-and-down (“painting technique”)<sup>48,53</sup> across a  $\sim 120$   $\mu\text{m}$  pinhole aperture in a Teflon septum separating two compartments containing 1.3 mL of electrolyte buffer solutions (symmetrical conditions: 250 mM KCl, 10 mM MOPS/Tris, pH 7.2 in *cis* and *trans* chambers; for asymmetrical conditions, the electrolyte solution in the *trans* chamber was replaced by perfusion to 20 mM KCl, 10 mM MOPS/Tris, pH 7.2). BLM formation was verified visually using a built-in low-amplification microscope and by checking capacitance measurements. Only stable, low conductance (50–70 pS), low-noise (<15 pS) membranes were used for experiments, which generally lasted for around 2 h. After data recording, the well-characterized bacterial porin  $\alpha$ -hemolysin from *Staphylococcus aureus* was tested as a positive control, with channel ionic activity confirming integrity of the bilayer and proper functioning of the electrophysiology setup. For the electrophysiology experiments involving aggregation inhibitor compounds, we carried out preliminary studies to ensure that, at the tested concentrations, none of the compounds caused bilayer instability when added alone to the chamber buffer (instability being defined as a variation from baseline conductance).

Following at least 15 min to ensure the above BLM criteria,  $\alpha\text{S}$  oligomer preparation (1  $\mu\text{M}$ , in equivalent moles of monomeric  $\alpha\text{S}$ ) was added directly into the buffer solution in the *cis* compartment, just below the bilayer. Current traces were initially recorded at  $\pm 50$  mV in voltage clamp mode. Both chambers were equipped with magnetic stirrers to facilitate protein reconstitution into the BLM; stirring was activated by the Compact workstation for 30 s if the conductance threshold indicating pore formation (>70 pS) was not reached. In the event of pore formation, a recording protocol to characterize the pore electrophysiologically was automatically initiated by Patchmaster software (HEKA, Germany). The protocol consisted of the following: (i) voltage-ramping from  $-60$  mV to  $+60$  mV over 10 s, and vice versa; (ii) square wave-voltage pulses of  $-60$ ,  $-50$ ,  $-40$ ,  $-30$ ,  $-20$ ,  $-10$ ,  $0$ ,  $+10$ ,  $+20$ ,  $+30$ ,  $+40$ ,  $+50$ ,  $+60$  mV, with 10 s recording at each voltage; (iii) 100 s runs of recordings at  $\pm 40$  mV potential, repeated for three times. Applied voltages greater than  $\pm 60$  mV tended to cause IM-type bilayer instability. Ion selectivity was determined by changing to an asymmetrical salt concentration (250:20 mM KCl, *cis:trans*) to enable measurement of the reversal potential (membrane voltage for zero current). All electrophysiology experiments were performed at room temperature. Data files were converted using ABF utility ([www.synaptosoft.com](http://www.synaptosoft.com)) and processed using Clampfit 10 (Molecular Devices). Further statistical analysis was done using Microsoft Excel 2010 and GraphPad Prism 6.

#### Calculation of Pore Diameter Using Channel Conductance.

The pore size diameter can be readily estimated using the measured channel conductance, assuming a simplified cylindrical nanopore.<sup>21</sup> Pore diameter ( $2r$ ) is calculated in an electrolyte solution of defined conductivity ( $\sigma$ , 29.1 mS/cm for 250 mM KCl at 25 °C), for a membrane-spanning pore length ( $L$ , 7 nm for mitochondrial membranes) and ionic conductance ( $G$ ), according to the following equations:

$$r = r_0 [1 + (1 + 4L/\pi r_0)^{1/2}] \quad (1)$$

$$r_0 = G/4\sigma \quad (2)$$

**Vesicle Binding Studies Using Confocal Single-Particle Fluorescence Spectroscopy.** To characterize the binding of  $\alpha\text{S}$  oligomers with CL, single-molecule spectroscopy techniques were

applied. By labeling  $\alpha\text{S}$  and LUVs with fluorophores having two different excitation wavelengths (“red” for the peptide and “green” for the lipid), FCS enables the monitoring of interactions between the two particles.<sup>63</sup> Recombinant  $\alpha\text{S}$  was labeled with the fluorescent dye Alexa Fluor-647-succinimidylester (Thermo Fischer Scientific, U.S.A.) by mixing in a 1:2 ratio and incubating for 12 h at 4 °C. Unbound fluorophores were separated by two filtration steps using PD10 columns (Amersham Biosciences, Munich, Germany) equilibrated with 50 mM Tris-Cl buffer (pH 7.0). LUVs with IM-type and L-type membrane compositions (see above) were prepared as described previously.<sup>40</sup> Following evaporation of the chloroform by a gentle stream of  $\text{N}_2$  gas, the dried lipid mixture was rehydrated by mixing with 1 mL of 50  $\mu\text{M}$  Alexa Fluor-488 dye (Invitrogen, Thermo Fisher Scientific, U.S.A.) in 50 mM Tris-Cl buffer (pH 7.0) at room temperature. After the hydrated lipid suspension were vigorously vortexed, they were subjected to five freeze–thaw cycles by alternately placing the sample tubes in liquid nitrogen and an Eppendorf Thermomixer set at 20 °C. The lipid suspensions were then diluted to 1 mM with 50 mM Tris, and 500  $\mu\text{L}$  of the lipid suspensions was extruded through a 100 nm polycarbonate filter for 21 times. LUV fractions were run on a size-exclusion chromatography column using Sephadex G-200 to remove the free fluorescent dye molecules. A vesicle diameter of  $\sim 100$  nm was confirmed with dynamic light scattering measurements using a Zetasizer NanoZS (Malvern Instruments, Herrenberg, Germany). Vesicles were immediately utilized or kept at 4 °C and used within 48 h. Oligomer formation was induced by coincubating labeled  $\alpha\text{S}$  (diluted to 10–20 nM in 50 mM Tris, pH 7.0) with 10  $\mu\text{M}$   $\text{Fe}^{3+}$  for 20 min at room temperature. It has already been shown that attachment of the Alexa-647 label to  $\alpha\text{S}$  influences neither the oligomerization of the protein nor the binding of  $\alpha\text{S}$  to the vesicles.<sup>49</sup> Subsequently, LUVs were added at a final lipid concentration of 10  $\mu\text{M}$ . Measurements were carried out using an Insight Reader (Evotec Technologies, Hamburg, Germany) with dual color excitation at 488 and 633 nm. Five independent measurements were performed on four replicates per measurement group. Measurement time was 60 s for FCS and 10 s for SIFT. All measurements were performed at room temperature in 384-well glass-bottom sample plates (Greiner Bio-One, Solingen, Germany).

Data of scanned measurements were directly visualized in 2D-FIDA (fluorescence intensity distribution analysis) histograms (photon counting histograms). Photons were summed over time intervals of constant length, using a bin length of 40  $\mu\text{s}$ . Depicted histograms contain all photons of all consecutive measurements of one sample. To determine oligomer binding to vesicles, a four-component fit was used. The following values were fixed:  $Q_{\text{monomer}}$  in the red channel for component one,  $Q_{\text{oligomer}}$  in the red channel for component two,  $Q_{\text{vesicle}}$  in the green channel for components three and four. A free fit of brightness for bound  $\alpha\text{S}$  was calculated for the fourth component in the red channel. The brightness  $I$  was calculated using the following equation:  $I = C \times Q$ , where  $C$  = concentration of particles and  $Q$  = particle brightness. Thus,  $I/I_{\text{total}(\text{red})}$  is equivalent to the fraction of  $\alpha\text{S}$  bound to vesicles. The fraction of vesicles with bound  $\alpha\text{S}$  is equivalent to  $I/I_{\text{total}(\text{green})}$ . Data was analyzed using the software packages FCS+Plus Analyze and SIFT-2D Version 2c (Evotec Technologies, Hamburg, Germany) as previously described.<sup>50,65</sup>

**Mitochondrial Swelling Assay.** Mitochondria were freshly isolated from SH-SY5Y neuroblastoma cells as described in Camilleri et al.<sup>40</sup> The mitochondrial pellet was resuspended in mitochondrial buffer (MB: 10 mM HEPES, 5 mM succinate, 250 mM sucrose, 1 mM ATP, 0.08 mM ADP, 2 mM  $\text{K}_2\text{HPO}_4$ , 1 mM DTT, pH 7.5) and brought to 0.5–1 mg/mL of protein. Swelling was initiated by adding native or oligomeric  $\alpha\text{S}$ , 500  $\mu\text{M}$   $\text{Ca}^{2+}$ , or other swelling agent in a 96-well plate in a total volume of 100  $\mu\text{L}$ /well. Mitochondrial swelling was evaluated by following changes in the absorbance of the mitochondrial suspension at 540 nm ( $A_{540}$ ) every 5 min for 60 min.<sup>98</sup> In the case of swollen mitochondria, light transmission is increased (i.e., a reduced turbidity). This is measured as a decrease in the relative absorbance at  $A_{540}$ .<sup>99,100</sup> All measurements were performed at room temperature. After subtracting the blank (buffer

alone) from all values, mitochondrial swelling curves were graphed using Graphpad Prism.

**Determination of Cyto c Release from Isolated Mitochondria by Immunoblotting.** Aliquots of isolated mitochondria (20  $\mu\text{g}$ ) were incubated with  $\alpha\text{S}$  oligomers for 1 h at 30 °C in 1 $\times$  MB. The mitochondrial suspensions were then centrifuged at 16 000g for 10 min at 4 °C to pellet mitochondria. Equal aliquots of the supernatant were run on 4–16% Bis-Tris gradient gels (Life Technologies, Thermo Fischer Scientific, U.S.A.).<sup>101</sup> Proteins were electro-transferred to Hybond-ECL membrane (Amersham Biosciences, Munich, Germany), and the membrane was blocked overnight at 4 °C in 5% nonfat dry milk in TBS-T (Tris-buffered saline, 0.05% Tween-20). After the membrane was rinsed with TBS-T buffer, cyto c was immunostained with primary anticytochrome c antibody (Invitrogen) (1:1000 in TBS-T) plus secondary antimouse antibody bound to horseradish peroxidase (Sigma-Aldrich) (1:4000 dilution in TBS-T). Peroxidase activity was detected using the enhanced chemiluminescence ECL Prime kit (Amersham Biosciences, Munich, Germany) followed by autoradiography. The intensity of the cyt c bands was analyzed densitometrically using ImageJ Software (NIH Image).

**NAO-CL Binding Assay.** Binding of the fluorescent dye NAO to CL results in dimerization of the dye in a stacking organization; when dye molecules are brought in close proximity, the emitted fluorescence shifts from 525 nm for the monomer, to 640 nm for the dimer.<sup>72</sup> Phospholipids (2  $\mu\text{M}$ ) were pipetted into 96-well half-area clear-bottom black plates, and NAO (0.5  $\mu\text{M}$ ) was added. To test for  $\alpha\text{S}$ -CL binding,  $\alpha\text{S}$  protein samples were incubated for 1 h with CL before addition of NAO. The incubation time of NAO with CL or the PLs was about 15 min in the darkness. The total volume of each well was 200  $\mu\text{L}$ , and samples were measured in quadruplicate using a Bio-Tek FLx800 fluorescence microplate reader (Bio-Tek, Germany).

**Statistical Analysis.** Data are displayed as mean  $\pm$  standard error of the mean (SEM) unless stated otherwise, with  $n$  as the number of independent experiments. Normal distribution of data was evaluated by D'Agostino-Pearson normality test. Differences between means were determined by one-tailed Student's  $t$ -test for pairwise comparisons and by one-way ANOVA followed by Bonferroni posthoc adjustment for multiple comparisons. Significance was determined at an  $\alpha$ -level of  $p < 0.05$ . Statistical analyses were performed using the software package GraphPad Prism v6 (GraphPad Software, San Diego, CA, U.S.A.) or Microsoft Excel 2016 (Microsoft Corporation, Redmond, WA, U.S.A.).

## ■ ASSOCIATED CONTENT

### ● Supporting Information

The Supporting Information is available free of charge on the ACS Publications website at DOI: 10.1021/acschemneur.9b00320.

Formation of higher-order  $\alpha\text{S}$  oligomers by ferric ions, latency to first opening after addition of  $\alpha\text{S}$  oligomeric preparation, histogram of conductance steps of  $\alpha\text{S}$  pores in IM-type bilayers, and segment representation in 2D-FIDA histograms (PDF)

## ■ AUTHOR INFORMATION

### Corresponding Author

\*Telephone: +356-2340-3294. E-mail: [neville.vassallo@um.edu.mt](mailto:neville.vassallo@um.edu.mt).

### ORCID

Viktoria C. Ruf: 0000-0002-3876-8854

Christian Griesinger: 0000-0002-1266-4344

Frits Kamp: 0000-0001-8382-6884

Neville Vassallo: 0000-0002-8985-5587

### Author Contributions

N.V., A.G., R.J.C., S.G., and A.C. conceived and designed the experiments; S.G., A.C., and M.C. performed the experiments;

A.C., S.G., A.G., R.J.C., and N.V. analyzed the data; F.K., V.R., F.S., A.L., S.R., and C.G. contributed reagents/materials/analysis tools. N.V. and S.G. wrote the paper.

### Funding

This work was supported in the main by a grant from the Malta Council for Science & Technology (MCST) through the National Research & Innovation Programme to RC and NV (R&I-2012-066). Additional funding support was obtained from the University of Malta (MDSIN08-21 and PHBR06 to NV). Work at the Ludwig-Maximilians-University of Munich was funded by internal resources. AC was supported by a scholarship grant awarded by the Malta Government Scholarship Scheme. MC was supported by a Research Officer Fellowship from the Faculty of Medicine and Surgery, University of Malta.

### Notes

The authors declare the following competing financial interest(s): A.G. and C.G. are co-inventors in a patent application related to the anle138b compound included in this study. A.G. and C.G. are shareholders and co-founders of MODAG GmbH. A.L. is currently partly employed by MODAG. All the other authors have no conflict of interest to declare.

## ■ ABBREVIATIONS

$\alpha\text{S}$ , alpha-synuclein; BLM, bilayer membrane; BTE, black tea extract; CL, cardiolipin; cyto c, cytochrome c; DIDS, 4,4'-diisothiocyanostilbene-2,2'-disulfonic acid; FCS, fluorescence correlation spectroscopy; FIDA, fluorescence intensity distribution analysis; IMM, inner mitochondrial membrane; LUVs, large unilamellar vesicles; NAO, 10-N-nonyl acridine orange; OMM, outer mitochondrial membrane; PD, Parkinson's disease; SIFT, scanning for intensely fluorescent targets; VDAC, voltage-dependent anion channel.

## ■ REFERENCES

- (1) Lees, A. J., Hardy, J., and Revesz, T. (2009) Parkinson's disease. *Lancet* 373, 2055–2066.
- (2) Shults, C. W. (2006) Lewy bodies. *Proc. Natl. Acad. Sci. U. S. A.* 103, 1661–1668.
- (3) Eschbach, J., and Danzer, K. M. (2014) alpha-Synuclein in Parkinson's disease: pathogenic function and translation into animal models. *Neurodegener. Dis.* 14, 1–17.
- (4) Wong, Y. C., and Krainc, D. (2017) alpha-synuclein toxicity in neurodegeneration: mechanism and therapeutic strategies. *Nat. Med.* 23, 1–13.
- (5) Comellas, G., Lemkau, L. R., Zhou, D. H., George, J. M., and Rienstra, C. M. (2012) Structural intermediates during alpha-synuclein fibrillogenesis on phospholipid vesicles. *J. Am. Chem. Soc.* 134, 5090–5099.
- (6) Stockl, M., Claessens, M. M., and Subramaniam, V. (2012) Kinetic measurements give new insights into lipid membrane permeabilization by alpha-synuclein oligomers. *Mol. BioSyst.* 8, 338–345.
- (7) Lorenzen, N., Nielsen, S. B., Buell, A. K., Kaspersen, J. D., Arosio, P., Vad, B. S., Paslawski, W., Christiansen, G., Valnickova-Hansen, Z., Andreasen, M., Enghild, J. J., Pedersen, J. S., Dobson, C. M., Knowles, T. P., and Otzen, D. E. (2014) The role of stable alpha-synuclein oligomers in the molecular events underlying amyloid formation. *J. Am. Chem. Soc.* 136, 3859–3868.
- (8) Demuro, A., Mina, E., Kaye, R., Milton, S. C., Parker, I., and Glabe, C. G. (2005) Calcium dysregulation and membrane disruption as a ubiquitous neurotoxic mechanism of soluble amyloid oligomers. *J. Biol. Chem.* 280, 17294–17300.

- (9) Furukawa, K., Matsuzaki-Kobayashi, M., Hasegawa, T., Kikuchi, A., Sugeno, N., Itoyama, Y., Wang, Y., Yao, P. J., Bushlin, L., and Takeda, A. (2006) Plasma membrane ion permeability induced by mutant alpha-synuclein contributes to the degeneration of neural cells. *J. Neurochem.* 97, 1071–1077.
- (10) Roberts, H. L., and Brown, D. R. (2015) Seeking a mechanism for the toxicity of oligomeric alpha-synuclein. *Biomolecules* 5, 282–305.
- (11) Angelova, P. R., Ludtmann, M. H., Horrocks, M. H., Negoda, A., Cremades, N., Klenerman, D., Dobson, C. M., Wood, N. W., Pavlov, E. V., Gandhi, S., and Abramov, A. Y. (2016) Ca<sup>2+</sup> is a key factor in alpha-synuclein-induced neurotoxicity. *J. Cell Sci.* 129, 1792–1801.
- (12) Winner, B., Jappelli, R., Maji, S. K., Desplats, P. A., Boyer, L., Aigner, S., Hetzer, C., Lohr, T., Vilar, M., Campioni, S., Tzitzilonis, C., Soragni, A., Jessberger, S., Mira, H., Consiglio, A., Pham, E., Masliah, E., Gage, F. H., and Riek, R. (2011) In vivo demonstration that alpha-synuclein oligomers are toxic. *Proc. Natl. Acad. Sci. U. S. A.* 108, 4194–4199.
- (13) Snead, D., and Eliezer, D. (2014) Alpha-synuclein function and dysfunction on cellular membranes. *Exp. Neurobiol.* 23, 292–313.
- (14) Sokolov, Y., Kozak, J. A., Kaye, R., Chanturiya, A., Glabe, C., and Hall, J. E. (2006) Soluble amyloid oligomers increase bilayer conductance by altering dielectric structure. *J. Gen. Physiol.* 128, 637–647.
- (15) Ouberai, M. M., Wang, J., Swann, M. J., Galvagnion, C., Guilliams, T., Dobson, C. M., and Welland, M. E. (2013) alpha-Synuclein senses lipid packing defects and induces lateral expansion of lipids leading to membrane remodeling. *J. Biol. Chem.* 288, 20883–20895.
- (16) Reynolds, N. P., Soragni, A., Rabe, M., Verdes, D., Liverani, E., Handschin, S., Riek, R., and Seeger, S. (2011) Mechanism of membrane interaction and disruption by alpha-synuclein. *J. Am. Chem. Soc.* 133, 19366–19375.
- (17) Hellstrand, E., Nowacka, A., Topgaard, D., Linse, S., and Sparr, E. (2013) Membrane lipid co-aggregation with alpha-synuclein fibrils. *PLoS One* 8, e77235.
- (18) van Maarschalkerweerd, A., Vetri, V., Langkilde, A. E., Fodera, V., and Vestergaard, B. (2014) Protein/lipid coaggregates are formed during alpha-synuclein-induced disruption of lipid bilayers. *Biomacromolecules* 15, 3643–3654.
- (19) Zakharov, S. D., Hulleman, J. D., Dutseva, E. A., Antonenko, Y. N., Rochet, J. C., and Cramer, W. A. (2007) Helical alpha-synuclein forms highly conductive ion channels. *Biochemistry* 46, 14369–14379.
- (20) Kim, H. Y., Cho, M. K., Kumar, A., Maier, E., Siebenhaar, C., Becker, S., Fernandez, C. O., Lashuel, H. A., Benz, R., Lange, A., and Zweckstetter, M. (2009) Structural properties of pore-forming oligomers of alpha-synuclein. *J. Am. Chem. Soc.* 131, 17482–17489.
- (21) Tosatto, L., Andrighetti, A. O., Plotegher, N., Antonini, V., Tessari, I., Ricci, L., Bubacco, L., and Dalla Serra, M. (2012) Alpha-synuclein pore forming activity upon membrane association. *Biochim. Biophys. Acta, Biomembr.* 1818, 2876–2883.
- (22) Quist, A., Doudevski, I., Lin, H., Azimova, R., Ng, D., Frangione, B., Kagan, B., Ghiso, J., and Lal, R. (2005) Amyloid ion channels: a common structural link for protein-misfolding disease. *Proc. Natl. Acad. Sci. U. S. A.* 102, 10427–10432.
- (23) Zhang, H., Griggs, A., Rochet, J. C., and Stanciu, L. A. (2013) In vitro study of alpha-synuclein protofibrils by cryo-EM suggests a Cu(2+)-dependent aggregation pathway. *Biophys. J.* 104, 2706–2713.
- (24) Giehm, L., Svergun, D. I., Otzen, D. E., and Vestergaard, B. (2011) Low-resolution structure of a vesicle disrupting alpha-synuclein oligomer that accumulates during fibrillation. *Proc. Natl. Acad. Sci. U. S. A.* 108, 3246–3251.
- (25) Tsigelny, I. F., Sharikov, Y., Miller, M. A., and Masliah, E. (2008) Mechanism of alpha-synuclein oligomerization and membrane interaction: theoretical approach to unstructured proteins studies. *Nanomedicine* 4, 350–357.
- (26) Tsigelny, I. F., Sharikov, Y., Wrasidlo, W., Gonzalez, T., Desplats, P. A., Crews, L., Spencer, B., and Masliah, E. (2012) Role of alpha-synuclein penetration into the membrane in the mechanisms of oligomer pore formation. *FEBS J.* 279, 1000–1013.
- (27) Middleton, E. R., and Rhoades, E. (2010) Effects of curvature and composition on alpha-synuclein binding to lipid vesicles. *Biophys. J.* 99, 2279–2288.
- (28) Pfefferkorn, C. M., Jiang, Z., and Lee, J. C. (2012) Biophysics of alpha-synuclein membrane interactions. *Biochim. Biophys. Acta, Biomembr.* 1818, 162–171.
- (29) Stockl, M., Fischer, P., Wanker, E., and Herrmann, A. (2008) Alpha-synuclein selectively binds to anionic phospholipids embedded in liquid-disordered domains. *J. Mol. Biol.* 375, 1394–1404.
- (30) van Rooijen, B. D., Claessens, M. M., and Subramaniam, V. (2009) Lipid bilayer disruption by oligomeric alpha-synuclein depends on bilayer charge and accessibility of the hydrophobic core. *Biochim. Biophys. Acta, Biomembr.* 1788, 1271–1278.
- (31) Stefanovic, A. N., Stockl, M. T., Claessens, M. M., and Subramaniam, V. (2014) alpha-Synuclein oligomers distinctively permeabilize complex model membranes. *FEBS J.* 281, 2838–2850.
- (32) Pirc, K., and Ulrih, N. P. (2015) alpha-Synuclein interactions with phospholipid model membranes: Key roles for electrostatic interactions and lipid-bilayer structure. *Biochim. Biophys. Acta, Biomembr.* 1848, 2002–2012.
- (33) Pacelli, C., Giguere, N., Bourque, M. J., Levesque, M., Slack, R. S., and Trudeau, L. E. (2015) Elevated Mitochondrial Bioenergetics and Axonal Arborization Size Are Key Contributors to the Vulnerability of Dopamine Neurons. *Curr. Biol.* 25, 2349–2360.
- (34) Ardail, D., Privat, J. P., Egret-Charlier, M., Levrat, C., Lerme, F., and Louisot, P. (1990) Mitochondrial contact sites. Lipid composition and dynamics. *J. Biol. Chem.* 265, 18797–18802.
- (35) Horvath, S. E., and Daum, G. (2013) Lipids of mitochondria. *Prog. Lipid Res.* 52, 590–614.
- (36) Elias-Wolff, F., Linden, M., Lyubartsev, A. P., and Brandt, E. G. (2019) Curvature sensing by cardiolipin in simulated buckled membranes. *Soft Matter* 15, 792–802.
- (37) Claypool, S. M. (2009) Cardiolipin, a critical determinant of mitochondrial carrier protein assembly and function. *Biochim. Biophys. Acta, Biomembr.* 1788, 2059–2068.
- (38) Paradies, G., Paradies, V., De Benedictis, V., Ruggiero, F. M., and Petrosillo, G. (2014) Functional role of cardiolipin in mitochondrial bioenergetics. *Biochim. Biophys. Acta, Bioenerg.* 1837, 408–417.
- (39) Ellis, C. E., Murphy, E. J., Mitchell, D. C., Golovko, M. Y., Scaglia, F., Barcelo-Coblijn, G. C., and Nussbaum, R. L. (2005) Mitochondrial lipid abnormality and electron transport chain impairment in mice lacking alpha-synuclein. *Mol. Cell. Biol.* 25, 10190–10201.
- (40) Camilleri, A., Zarb, C., Caruana, M., Ostermeier, U., Ghio, S., Hogen, T., Schmidt, F., Giese, A., and Vassallo, N. (2013) Mitochondrial membrane permeabilisation by amyloid aggregates and protection by polyphenols. *Biochim. Biophys. Acta, Biomembr.* 1828, 2532–2543.
- (41) Ghio, S., Kamp, F., Cauchi, R., Giese, A., and Vassallo, N. (2016) Interaction of alpha-synuclein with biomembranes in Parkinson's disease—role of cardiolipin. *Prog. Lipid Res.* 61, 73–82.
- (42) Robotta, M., Gerding, H. R., Vogel, A., Hauser, K., Schildknecht, S., Karreman, C., Leist, M., Subramaniam, V., and Drescher, M. (2014) Alpha-synuclein binds to the inner membrane of mitochondria in an alpha-helical conformation. *ChemBioChem* 15, 2499–2502.
- (43) Shen, J., Du, T., Wang, X., Duan, C., Gao, G., Zhang, J., Lu, L., and Yang, H. (2014) alpha-Synuclein amino terminus regulates mitochondrial membrane permeability. *Brain Res.* 1591, 14–26.
- (44) Devi, L., Raghavendran, V., Prabhu, B. M., Avadhani, N. G., and Anandatheerthavarada, H. K. (2008) Mitochondrial import and accumulation of alpha-synuclein impair complex I in human dopaminergic neuronal cultures and Parkinson disease brain. *J. Biol. Chem.* 283, 9089–9100.
- (45) Maldonado Vidaurri, E., Chavez-Montes, A., Garza Tapia, M., Castro-Rios, R., and Gonzalez-Horta, A. (2018) Differential

interaction of alpha-synuclein N-terminal segment with mitochondrial model membranes. *Int. J. Biol. Macromol.* 119, 1286–1293.

(46) Camilleri, A., and Vassallo, N. (2014) The centrality of mitochondria in the pathogenesis and treatment of Parkinson's disease. *CNS Neurosci. Ther.* 20, 591–602.

(47) Marom, M., and Azem, A. (2013) The use of cardiolipin-containing liposomes as a model system to study the interaction between proteins and the inner mitochondrial membrane. *Methods Mol. Biol.* 1033, 147–155.

(48) Schmidt, F., Levin, J., Kamp, F., Kretzschmar, H., Giese, A., and Botzel, K. (2012) Single-channel electrophysiology reveals a distinct and uniform pore complex formed by alpha-synuclein oligomers in lipid membranes. *PLoS One* 7, e42545.

(49) Kostka, M., Hogen, T., Danzer, K. M., Levin, J., Habeck, M., Wirth, A., Wagner, R., Glabe, C. G., Finger, S., Heinzlmann, U., Garidel, P., Duan, W., Ross, C. A., Kretzschmar, H., and Giese, A. (2008) Single particle characterization of iron-induced pore-forming alpha-synuclein oligomers. *J. Biol. Chem.* 283, 10992–11003.

(50) Ruf, V., Nubling, G. S., Willikens, S., Shi, S., Schmidt, F., Levin, J., Botzel, K., Kamp, F., and Giese, A. (2019) Different effects of alpha-synuclein mutants on lipid binding and aggregation detected by single molecule fluorescence spectroscopy and ThT fluorescence-based measurements. *ACS Chem. Neurosci.* 10, 1649.

(51) Danzer, K. M., Haasen, D., Karow, A. R., Moussaud, S., Habeck, M., Giese, A., Kretzschmar, H., Hengerer, B., and Kostka, M. (2007) Different species of alpha-synuclein oligomers induce calcium influx and seeding. *J. Neurosci.* 27, 9220–9232.

(52) Huls, S., Hogen, T., Vassallo, N., Danzer, K. M., Hengerer, B., Giese, A., and Herms, J. (2011) AMPA-receptor-mediated excitatory synaptic transmission is enhanced by iron-induced alpha-synuclein oligomers. *J. Neurochem.* 117, 868–878.

(53) Gutschmann, T., Heimbürg, T., Keyser, U., Mahendran, K. R., and Winterhalter, M. (2015) Protein reconstitution into freestanding planar lipid membranes for electrophysiological characterization. *Nat. Protoc.* 10, 188–198.

(54) Krüger, V., Deckers, M., Hildenbeutel, M., van der Laan, M., Hellmers, M., Dreker, C., Preuss, M., Herrmann, J. M., Rehling, P., Wagner, R., and Meinecke, M. (2012) The mitochondrial oxidase assembly protein1 (Oxa1) insertase forms a membrane pore in lipid bilayers. *J. Biol. Chem.* 287, 33314–33326.

(55) Wagner, J., Ryazanov, S., Leonov, A., Levin, J., Shi, S., Schmidt, F., Prix, C., Pan-Montojo, F., Bertsch, U., Mitteregger-Kretzschmar, G., Geissen, M., Eiden, M., Leidel, F., Hirschberger, T., Deeg, A. A., Krauth, J. J., Zinth, W., Tavan, P., Pilger, J., Zweckstetter, M., Frank, T., Bahr, M., Weishaupt, J. H., Uhr, M., Urlaub, H., Teichmann, U., Samwer, M., Botzel, K., Groschup, M., Kretzschmar, H., Griesinger, C., and Giese, A. (2013) Anle138b: a novel oligomer modulator for disease-modifying therapy of neurodegenerative diseases such as prion and Parkinson's disease. *Acta Neuropathol.* 125, 795–813.

(56) Deeg, A. A., Reiner, A. M., Schmidt, F., Schueder, F., Ryazanov, S., Ruf, V. C., Giller, K., Becker, S., Leonov, A., Griesinger, C., Giese, A., and Zinth, W. (2015) Anle138b and related compounds are aggregation specific fluorescence markers and reveal high affinity binding to alpha-synuclein aggregates. *Biochim. Biophys. Acta, Gen. Subj.* 1850, 1884–1890.

(57) Matthes, D., Gapsys, V., Griesinger, C., and de Groot, B. L. (2017) Resolving the Atomistic Modes of Anle138b Inhibitory Action on Peptide Oligomer Formation. *ACS Chem. Neurosci.* 8, 2791–2808.

(58) Caruana, M., Hogen, T., Levin, J., Hillmer, A., Giese, A., and Vassallo, N. (2011) Inhibition and disaggregation of alpha-synuclein oligomers by natural polyphenolic compounds. *FEBS Lett.* 585, 1113–1120.

(59) Grelle, G., Otto, A., Lorenz, M., Frank, R. F., Wanker, E. E., and Bieschke, J. (2011) Black tea theaflavins inhibit formation of toxic amyloid-beta and alpha-synuclein fibrils. *Biochemistry* 50, 10624–10636.

(60) Caruana, M., and Vassallo, N. (2015) Tea Polyphenols in Parkinson's Disease. *Adv. Exp. Med. Biol.* 863, 117–137.

(61) Sigworth, F. J., and Sine, S. M. (1987) Data transformations for improved display and fitting of single-channel dwell time histograms. *Biophys. J.* 52, 1047–1054.

(62) Takamori, S., Holt, M., Stenius, K., Lemke, E. A., Grønborg, M., Riedel, D., Urlaub, H., Schenck, S., Brügger, B., Ringler, P., Müller, S. A., Rammner, B., Gräter, F., Hub, J. S., De Groot, B. L., Mieskes, G., Moriyama, Y., Klingauf, J., Grubmüller, H., Heuser, J., Wieland, F., and Jahn, R. (2006) Molecular anatomy of a trafficking organelle. *Cell* 127, 831–846.

(63) Giese, A., Bader, B., Bieschke, J., Schaffar, G., Odoy, S., Kahle, P. J., Haass, C., and Kretzschmar, H. (2005) Single particle detection and characterization of synuclein co-aggregation. *Biochem. Biophys. Res. Commun.* 333, 1202–1210.

(64) Bader, B., Nubling, G., Mehle, A., Nobile, S., Kretzschmar, H., and Giese, A. (2011) Single particle analysis of tau oligomer formation induced by metal ions and organic solvents. *Biochem. Biophys. Res. Commun.* 411, 190–196.

(65) Nubling, G. S., Levin, J., Bader, B., Lorenz, S., Hillmer, A., Hogen, T., Kamp, F., and Giese, A. (2014) Modelling Ser129 phosphorylation inhibits membrane binding of pore-forming alpha-synuclein oligomers. *PLoS One* 9, e98906.

(66) Tait, S. W., and Green, D. R. (2013) Mitochondrial regulation of cell death. *Cold Spring Harb Perspect Biol.* 5, a008706.

(67) Gillies, L. A., and Kuwana, T. (2014) Apoptosis regulation at the mitochondrial outer membrane. *J. Cell. Biochem.* 115, 632–640.

(68) Petit, J. M., Maftah, A., Ratinaud, M. H., and Julien, R. (1992) 10-N-nonyl acridine orange interacts with cardiolipin and allows the quantification of this phospholipid in isolated mitochondria. *Eur. J. Biochem.* 209, 267–273.

(69) Zhang, G. X., Kimura, S., Murao, K., Obata, K., Matsuyoshi, H., and Takaki, M. (2010) Inhibition of cytochrome c release by 10-N-nonyl acridine orange, a cardiolipin-specific dye, during myocardial ischemia-reperfusion in the rat. *Am. J. Physiol. Heart Circ. Physiol.* 298, H433–439.

(70) Martinou, J. C., Desagher, S., and Antonsson, B. (2000) Cytochrome c release from mitochondria: all or nothing. *Nat. Cell Biol.* 2, E41–43.

(71) Ichimura, T., Ito, M., Takahashi, K., Oyama, K., and Sakurai, K. (2011) Involvement of mitochondrial swelling in cytochrome c release from mitochondria treated with calcium and Alloxan. *J. Biophys. Chem.* 02, 10–18.

(72) Kaewsuya, P., Danielson, N. D., and Ekhterae, D. (2007) Fluorescent determination of cardiolipin using 10-N-nonyl acridine orange. *Anal. Bioanal. Chem.* 387, 2775–2782.

(73) Birk, A. V., Liu, S., Soong, Y., Mills, W., Singh, P., Warren, J. D., Seshan, S. V., Pardee, J. D., and Szeto, H. H. (2013) The mitochondrial-targeted compound SS-31 re-energizes ischemic mitochondria by interacting with cardiolipin. *J. Am. Soc. Nephrol.* 24, 1250–1261.

(74) Martin, L. J., Pan, Y., Price, A. C., Sterling, W., Copeland, N. G., Jenkins, N. A., Price, D. L., and Lee, M. K. (2006) Parkinson's disease alpha-synuclein transgenic mice develop neuronal mitochondrial degeneration and cell death. *J. Neurosci.* 26, 41–50.

(75) Subramaniam, S. R., Vergnes, L., Franich, N. R., Reue, K., and Chesselet, M. F. (2014) Region specific mitochondrial impairment in mice with widespread overexpression of alpha-synuclein. *Neurobiol. Dis.* 70, 204–213.

(76) Reeve, A. K., Grady, J. P., Cosgrave, E. M., Bennison, E., Chen, C., Hepplewhite, P. D., and Morris, C. M. (2018) Mitochondrial dysfunction within the synapses of substantia nigra neurons in Parkinson's disease. *NPJ. Parkinsons Dis.* 4, 9.

(77) Azimov, R., and Kagan, B. (2015) Amyloid Peptide Channels. In *Electrophysiology of Unconventional Channels and Pores* (Delcour, A. H., Ed.) pp 343–360, Springer International Publishing, Basel, Switzerland.

(78) Xu, J., Vanderlick, T. K., and Beales, P. A. (2013) Lytic and non-lytic permeabilization of cardiolipin-containing lipid bilayers induced by cytochrome C. *PLoS One* 8, e69492.

- (79) Huang, H. W., Chen, F. Y., and Lee, M. T. (2004) Molecular mechanism of Peptide-induced pores in membranes. *Phys. Rev. Lett.* 92, 198304.
- (80) Kaye, R., Sokolov, Y., Edmonds, B., McIntire, T. M., Milton, S. C., Hall, J. E., and Glabe, C. G. (2004) Permeabilization of lipid bilayers is a common conformation-dependent activity of soluble amyloid oligomers in protein misfolding diseases. *J. Biol. Chem.* 279, 46363–46366.
- (81) Jang, H., Arce, F. T., Capone, R., Ramachandran, S., Lal, R., and Nussinov, R. (2009) Misfolded amyloid ion channels present mobile beta-sheet subunits in contrast to conventional ion channels. *Biophys. J.* 97, 3029–3037.
- (82) Tsigelny, I. F., Bar-On, P., Sharikov, Y., Crews, L., Hashimoto, M., Miller, M. A., Keller, S. H., Platoshyn, O., Yuan, J. X., and Masliah, E. (2007) Dynamics of alpha-synuclein aggregation and inhibition of pore-like oligomer development by beta-synuclein. *FEBS J.* 274, 1862–1877.
- (83) Gao, G., Wang, Z., Lu, L., Duan, C., Wang, X., and Yang, H. (2017) Morphological analysis of mitochondria for evaluating the toxicity of alpha-synuclein in transgenic mice and isolated preparations by atomic force microscopy. *Biomed. Pharmacother.* 96, 1380–1388.
- (84) Schauer, J. A., Wong, P. T., Wisser, K. C., Ding, H., Steel, D. G., and Gafni, A. (2010) Simultaneous single-molecule fluorescence and conductivity studies reveal distinct classes of Abeta species on lipid bilayers. *Biochemistry* 49, 3031–3039.
- (85) Luth, E. S., Stavrovskaya, I. G., Bartels, T., Kristal, B. S., and Selkoe, D. J. (2014) Soluble, prefibrillar alpha-synuclein oligomers promote complex I-dependent, Ca<sup>2+</sup>-induced mitochondrial dysfunction. *J. Biol. Chem.* 289, 21490–21507.
- (86) Domanska, G., Motz, C., Meinecke, M., Harsman, A., Papatheodorou, P., Reljic, B., Dian-Lothrop, E. A., Galmiche, A., Kepp, O., Becker, L., Gunnewig, K., Wagner, R., and Rassow, J. (2010) Helicobacter pylori VacA toxin/subunit p34: targeting of an anion channel to the inner mitochondrial membrane. *PLoS Pathog.* 6, e1000878.
- (87) Kozjak-Pavlovic, V., Dian-Lothrop, E. A., Meinecke, M., Kepp, O., Ross, K., Rajalingam, K., Harsman, A., Hauf, E., Brinkmann, V., Gunther, D., Herrmann, I., Hurwitz, R., Rassow, J., Wagner, R., and Rudel, T. (2009) Bacterial porin disrupts mitochondrial membrane potential and sensitizes host cells to apoptosis. *PLoS Pathog.* 5, e1000629.
- (88) Maftah, A., Petit, J. M., and Julien, R. (1990) Specific interaction of the new fluorescent dye 10-N-nonyl acridine orange with inner mitochondrial membrane. A lipid-mediated inhibition of oxidative phosphorylation. *FEBS Lett.* 260, 236–240.
- (89) Godard, A., Heymann, D., Rahe, S., Anegon, I., Peyrat, M. A., Le Mauff, B., Mouray, E., Gregoire, M., Virdee, K., Soullillou, J. P., et al. (1992) High and low affinity receptors for human interleukin for DA cells/leukemia inhibitory factor on human cells. Molecular characterization and cellular distribution. *J. Biol. Chem.* 267, 3214–3222.
- (90) Garcia Fernandez, M. I., Ceccarelli, D., and Muscatello, U. (2004) Use of the fluorescent dye 10-N-nonyl acridine orange in quantitative and location assays of cardiolipin: a study on different experimental models. *Anal. Biochem.* 328, 174–180.
- (91) Nakamura, K., Nemani, V. M., Azarbal, F., Skibinski, G., Levy, J. M., Egami, K., Munishkina, L., Zhang, J., Gardner, B., Wakabayashi, J., Sasaki, H., Cheng, Y., Finkbeiner, S., Nussbaum, R. L., Masliah, E., and Edwards, R. H. (2011) Direct membrane association drives mitochondrial fission by the Parkinson disease-associated protein alpha-synuclein. *J. Biol. Chem.* 286, 20710–20726.
- (92) Zigoneanu, I. G., Yang, Y. J., Krois, A. S., Haque, E., and Pielak, G. J. (2012) Interaction of alpha-synuclein with vesicles that mimic mitochondrial membranes. *Biochim. Biophys. Acta, Biomembr.* 1818, 512–519.
- (93) Ryan, T., Bamm, V. V., Stykel, M. G., Coackley, C. L., Humphries, K. M., Jamieson-Williams, R., Ambasudhan, R., Mosser, D. D., Lipton, S. A., Harauz, G., and Ryan, S. D. (2018) Cardiolipin exposure on the outer mitochondrial membrane modulates alpha-synuclein. *Nat. Commun.* 9, 817.
- (94) Lai, Y. C., Li, C. C., Sung, T. C., Chang, C. W., Lan, Y. J., and Chiang, Y. W. (2019) The role of cardiolipin in promoting the membrane pore-forming activity of BAX oligomers. *Biochim. Biophys. Acta, Biomembr.* 1861, 268–280.
- (95) Gasanov, S. E., Shrivastava, I. H., Israilov, F. S., Kim, A. A., Rylava, K. A., Zhang, B., and Dagda, R. K. (2015) Naja naja oxiana Cobra Venom Cytotoxins CTI and CTII Disrupt Mitochondrial Membrane Integrity: Implications for Basic Three-Fingered Cytotoxins. *PLoS One* 10, e0129248.
- (96) Martinez Hernandez, A., Urbanke, H., Gillman, A. L., Lee, J., Ryazanov, S., Agbemenyah, H. Y., Benito, E., Jain, G., Kaurani, L., Grigorian, G., Leonov, A., Rezaei-Ghaleh, N., Wilken, P., Arce, F. T., Wagner, J., Fuhrmann, M., Caruana, M., Camilleri, A., Vassallo, N., Zweckstetter, M., Benz, R., Giese, A., Schneider, A., Korte, M., Lal, R., Griesinger, C., Eichele, G., and Fischer, A. (2018) The diphenylpyrazole compound anle138b blocks Abeta channels and rescues disease phenotypes in a mouse model for amyloid pathology. *EMBO Mol. Med.* 10, 32–47.
- (97) Nuscher, B., Kamp, F., Mehnert, T., Odoy, S., Haass, C., Kahle, P. J., and Beyreuther, K. (2004) Alpha-synuclein has a high affinity for packing defects in a bilayer membrane: a thermodynamics study. *J. Biol. Chem.* 279, 21966–21975.
- (98) Milaeva, E. R., Filimonova, S. I., Meleshonkova, N. N., Dubova, L. G., Shevtsova, E. F., Bachurin, S. O., and Zefirov, N. S. (2010) Antioxidative activity of ferrocenes bearing 2,6-di-tert-butylphenol moieties. *Bioinorg Chem. Appl.* 2010, 165482.
- (99) Joiner, M. L., Koval, O. M., Li, J., He, B. J., Allamargot, C., Gao, Z., Luczak, E. D., Hall, D. D., Fink, B. D., Chen, B., Yang, J., Moore, S. A., Scholz, T. D., Strack, S., Mohler, P. J., Sivitz, W. I., Song, L. S., and Anderson, M. E. (2012) CaMKII determines mitochondrial stress responses in heart. *Nature* 491, 269–273.
- (100) Karch, J., Kwong, J. Q., Burr, A. R., Sargent, M. A., Elrod, J. W., Peixoto, P. M., Martinez-Caballero, S., Osinska, H., Cheng, E. H., Robbins, J., Kinnally, K. W., and Molkentin, J. D. (2013) Bax and Bak function as the outer membrane component of the mitochondrial permeability pore in regulating necrotic cell death in mice. *Elife* 2, e00772.
- (101) Gottlieb, E., Armour, S. M., Harris, M. H., and Thompson, C. B. (2003) Mitochondrial membrane potential regulates matrix configuration and cytochrome c release during apoptosis. *Cell Death Differ.* 10, 709–717.